The neutral kaon decays to $\pi^+\pi^-\pi^0$: a detailed analysis of the CPLEAR data

A. Angelopoulos, A. Apostolakis, E. Aslanides, G. Backenstoss, O. Behnke, A. Benelli, V. Bertin, F. Blanc, P. Bloch, P. Carlson, et al.

EUROPEAN ORGANIZATION FOR NUCLEAR RESEARCH

CERN–EP/98–74
13 March 1998

The neutral kaon decays to $\pi^+\pi^-\pi^0$: a detailed analysis of the CPLEAR data

CPLEAR Collaboration

A. Angelopoulos[1)], A. Apostolakis[1)], E. Aslanides[11)], G. Backenstoss[2)], P. Bargassa[13)], O. Behnke[17)], A. Benelli[2)], V. Bertin[11)], F. Blanc[7)], P. Bloch[4)], P. Carlson[15)], M. Carroll[9)], E. Cawley[9)], M.B. Chertok[3)], M. Danielsson[15)], M. Dejardin[14)], J. Derre[14)], A. Ealet[11)], C. Eleftheriadis[16)], L. Faravel[7)], P. Fassnacht[11)], W. Fetscher[17)], M. Fidecaro[4)], A. Filipčič[10)], D. Francis[3)], J. Fry[9)], E. Gabathuler[9)], R. Gamet[9)], H.-J. Gerber[17)], A. Go[4)], A. Haselden[9)], P.J. Hayman[9)], F. Henry-Couannier[11)], R.W. Hollander[6)], K. Jon-And[15)], P.-R. Kettle[13)], P. Kokkas[4)], R. Kreuger[6)], R. Le Gac[11)], F. Leimgruber[2)], I. Mandić[10)], N. Manthos[8)], G. Marel[14)], M. Mikuž[10)], J. Miller[3)], F. Montanet[11)], T. Nakada[13)], B. Pagels[17)], I. Papadopoulos[16)], P. Pavlopoulos[2)], G. Polivka[2)], R. Rickenbach[2)], B.L. Roberts[3)], T. Ruf[4)], M. Schäfer[17)], L.A. Schaller[7)], T. Schietinger[2)], A. Schopper[4)], L. Tauscher[2)], C. Thibault[12)], F. Touchard[11)], C. Touramanis[9)], C.W.E. Van Eijk[6)], S. Vlachos[2)], P. Weber[17)], O. Wigger[13)], M. Wolter[17)], D. Zavrtanik[10)] and D. Zimmerman[3)]

Abstract

A detailed analysis of neutral kaons decaying to $\pi^+\pi^-\pi^0$ is presented based on the complete data set containing half a million events. Time-dependent decay rate asymmetries are measured between initially tagged K^0 and $\overline{\mathrm{K}}^0$ and for different regions of the phase space. These asymmetries, resulting from the interference between the CP-conserving decay amplitude of $\mathrm{K_L}$ and the decay amplitude of $\mathrm{K_S}$ – either CP-violating or CP-conserving – allow the determination of the $\mathrm{K_S}$ parameters η_{+-0} (CP-violating) and λ (CP-conserving), and also of the main isospin components of the $\mathrm{K_S}$ decay amplitude. The branching ratio of $\mathrm{K_S} \to \pi^+\pi^-\pi^0$ (CP-conserving) is deduced directly from λ. In addition, we extract the slope parameters describing the energy dependence of the $\mathrm{K_L} \to \pi^+\pi^-\pi^0$ Dalitz plot. The whole set of our results fits well within the current phenomenological picture of the neutral-kaon system including CP violation and Chiral Perturbation Theory (ChPT).

(Submitted to European Physical Journal C)

1 Introduction

The CPLEAR experiment at the Low Energy Antiproton Ring at CERN uses a new experimental approach to study CP, T and CPT violation in neutral kaon decays. Neutral kaons, produced in $\overline{\mathrm{p}}\mathrm{p}$ (at rest) $\rightarrow \pi^+\mathrm{K}^-\mathrm{K}^0$ or $\pi^-\mathrm{K}^+\overline{\mathrm{K}}^0$, are initially strangeness tagged, event by event, and time-dependent decay-rate asymmetries between K^0 and $\overline{\mathrm{K}}^0$ are measured for decays to 2π, 3π and $\pi\mathrm{e}\nu_\mathrm{e}$. From these asymmetries the CP, T and CPT parameters – describing the violation of the corresponding symmetries in the neutral-kaon system – can be extracted with small systematic errors [1].

In this paper based on the analysis of our complete data set, we focus on the $\pi^+\pi^-\pi^0$ final state. The search for the CP-violating amplitude of $\mathrm{K_S} \rightarrow \pi^+\pi^-\pi^0$ decays is motivated by the search for CP violation itself, but the interest extends far beyond it. Recently the experimental precision in the measurement of the phase φ_{+-} of the CP-violating parameter η_{+-} was increased allowing for an improved indirect CPT test. To take full advantage of these new measurements, the precision of the CP-violating parameters of neutral kaons decaying to three pions also needs to be improved substantially [2, 3].

The measurement of the parameters η_{+-0}, describing the yet unobserved CP-violating $\mathrm{K_S}$ decay, and λ, describing the interference between the $\mathrm{K_S}$ and $\mathrm{K_L}$ CP-allowed amplitudes, is reported together with a detailed description of the method, the selection criteria and the systematic error estimation. In this framework we also present the measurement of the parameters describing the Dalitz distribution for $\mathrm{K_L} \rightarrow \pi^+\pi^-\pi^0$ and the determination of the CP-conserving $\mathrm{K_S} \rightarrow \pi^+\pi^-\pi^0$ amplitude in terms of its isospin components. The results on η_{+-0} and λ are already contained in a short version of this report [4].

In Section 2 we recall the conventional parametrization of the neutral-kaon decay amplitudes, and the definition of the CP-violating and CP-conserving parameters. In Section 3, we describe the experimental method applied to extract these parameters. The CPLEAR experiment is presented in Section 4, followed by the event selection and corrections in Section 5. The final results, obtained with the complete data set, are reported in Section 6, which is devoted to the measurement of the CP-violating and CP-conserving parameters, and in Section 7, devoted to the measurement of the isospin components of the $\mathrm{K_S}$ and $\mathrm{K_L}$ decay amplitudes and of the Dalitz-plot slope parameters. The CPLEAR contribution to the study of neutral-kaon decays to $\pi^+\pi^-\pi^0$ is summarized in Section 8.

[1] University of Athens, Greece
[2] University of Basle, Switzerland
[3] Boston University, USA
[4] CERN, Geneva, Switzerland
[5] LIP and University of Coimbra, Portugal
[6] Delft University of Technology, Netherlands
[7] University of Fribourg, Switzerland
[8] University of Ioannina, Greece
[9] University of Liverpool, UK
[10] J. Stefan Inst. and Phys. Dep., University of Ljubljana, Slovenia
[11] CPPM, IN2P3-CNRS et Université d'Aix-Marseille II, France
[12] CSNSM, IN2P3-CNRS, Orsay, France
[13] Paul Scherrer Institut (PSI), Switzerland
[14] CEA, DSM/DAPNIA, CE-Saclay, France
[15] Royal Institute of Technology, Stockholm, Sweden
[16] University of Thessaloniki, Greece
[17] ETH-IPP Zürich, Switzerland

2 Phenomenology of the neutral-kaon decay into $\pi^+\pi^-\pi^0$

The probability to find a given momentum configuration for the $\pi^+\pi^-\pi^0$ state is given by the Dalitz distribution function (Dalitz plot). It is often parametrized as a function of the Lorentz invariants X and Y. In the kaon rest frame X is proportional to the difference of the charged-pion energies and Y depends linearly on the neutral-pion energy. The definition of X and Y and the boundaries of the Dalitz plot are given in Section 2.1.

The Dalitz distribution is proportional to the modulus squared of the decay amplitude $A^{+-0}(X,Y)$. Its shape depends on the spin and the parity of the final state. As the sum of the masses of the three pions is close to the kaon mass, $A^{+-0}(X,Y)$ can be expanded as a polynomial in the relative momentum of the $\pi^+\pi^-$ subsystem and in the momentum of the π^0, or equivalently as a function of X and Y. In addition, the final state has to satisfy the Bose statistics requirement and be symmetric under the interchange of any two pions. Owing to these properties the general form of the neutral-kaon decay amplitude to $\pi^+\pi^-\pi^0$ is

$$A^{+-0}(X,Y) \propto 1 + a_1 Y + a_2 X + ...$$

Each term of the expansion is related to the angular momentum l of the π^0 relative to the $\pi^+\pi^-$ subsystem, and to the total isospin I.

A further variable is the CP eigenvalue of the final state, which depends on the angular momentum configuration of the three pions and is given by $(-1)^{l+1}$. Since K^0 and $\overline{\mathrm{K}}^0$ states are superpositions of the two physical states $\mathrm{K_S}$ and $\mathrm{K_L}$, four contributions to $A^{+-0}(X,Y)$ should be considered. Two of them come from the $\mathrm{K_S}$ and $\mathrm{K_L}$ decays to a $\pi^+\pi^-\pi^0$ state with $\mathrm{CP} = +1$ and two from the decay into a $\mathrm{CP} = -1$ state. The low kinetic energy available in the kaon rest frame suppresses high pion angular-momentum configurations. As a consequence, the $\mathrm{K}^0(\overline{\mathrm{K}}^0) \to \pi^+\pi^-\pi^0$ decay is strongly dominated by the $\mathrm{K_L}$ decay amplitude $(\mathrm{CP} = -1, l = 0)$, which is CP-allowed and kinematically favoured. The second contribution is due to the $\mathrm{K_S}$ decay amplitude $(\mathrm{CP} = +1, l = 1)$, which is CP-allowed and kinematically suppressed. Other contributions are expected from CP-violating $\mathrm{K_S}$ $(\mathrm{CP} = -1, l = 0)$ and $\mathrm{K_L}$ $(\mathrm{CP} = +1, l = 1)$ decay amplitudes. The latter is suppressed both by CP-violation and centrifugal effect and is thus neglected in most of this work. Three main contributions remain in the K^0 and $\overline{\mathrm{K}}^0$ decay amplitude:

$$A^{+-0}(X,Y) \;\approx\; A_{\mathrm{L}}^{3\pi\,(\mathrm{CP}=-1)}(X,Y) \pm [A_{\mathrm{S}}^{3\pi\,(\mathrm{CP}=+1)}(X,Y) + A_{\mathrm{S}}^{3\pi\,(\mathrm{CP}=-1)}(X,Y)],$$

where the upper and lower signs apply to K^0 and $\overline{\mathrm{K}}^0$, respectively.

The decomposition of each contribution as a function of I, l, X and Y is developed in Section 2.2, where we also define the Dalitz distribution observables in terms of the amplitude components. The observables describing the CP-conserving and CP-violating parts of the $\mathrm{K_S}$ decay amplitudes are defined in Section 2.3.

2.1 The Dalitz variables X and Y

The two Dalitz variables X and Y are defined as

$$X = \frac{s_{\pi^-} - s_{\pi^+}}{m^2_{\pi^\pm}} \quad \text{and} \quad Y = \frac{s_{\pi^0} - s_0}{m^2_{\pi^\pm}}\,,$$

where $m_{\pi^\pm}$ is the mass of the charged pion. The variables s_π are given by

$$s_\pi = (p_K - p_\pi)_\mu (p_K - p_\pi)^\mu\,,$$

where p_π and p_K are the four-momenta of the pion and the neutral kaon, respectively. The variable s_0 is defined as

$$s_0 = \frac{1}{3}\left(s_{\pi^+} + s_{\pi^-} + s_{\pi^0}\right).$$

The Dalitz variable Y varies in the range

$$Y_{\rm min} = 4 - \frac{s_0}{m^2_{\pi^\pm}} \quad \text{and} \quad Y_{\rm max} = 2\left(\frac{s_0}{m^2_{\pi^\pm}} - 1\right) - \sqrt{\left(3\frac{s_0}{m^2_{\pi^\pm}} - 2\right)^2 - \frac{(m^2_K - m^2_{\pi^0})^2}{m^4_{\pi^\pm}}}\ ,$$

while the kinematic limits for X are given by

$$X^2_{\rm lim}(Y) = Y^2 - 4\frac{s_0}{m^2_{\pi^\pm}}Y - \left(\frac{s_0}{m^2_{\pi^\pm}} - 4\right)\left(5\frac{s_0}{m^2_{\pi^\pm}} - 4\right) + \frac{(m^2_K - m^2_{\pi^0})^2}{m^4_{\pi^\pm}}\left(1 - \frac{4}{Y + s_0/m^2_{\pi^\pm}}\right).$$

2.2 Parametrization of the neutral-kaon decay amplitudes

We first recall that the $\pi^+\pi^-\pi^0$ final state, as any pion state, can be decomposed into a superposition of states with definite total isospin I. The amplitudes of a neutral kaon decaying to $\pi^+\pi^-\pi^0$ can be written as a sum of products containing the isospin, angular momentum and energy-momentum dependences [5]. Owing to the Bose statistics these amplitudes must be symmetric under the interchange of the π^0 with the π^+ or the π^- and of the π^+ with the π^-.

The total isospin I has a value between zero and three. For the angular momentum, we consider the relative angular momenta l_1 between the two charged pions, and l_2 between the $\pi^+\pi^-$ subsystem and the π^0. Owing to the zero spin of the neutral kaon, $l_1 = l_2 = l$. Therefore the $\pi^+\pi^-\pi^0$ state always corresponds to the eigenvalue -1 of the parity operator P. The eigenvalues of the operators C (charge-conjugation) and CP are $(-1)^l$ and $(-1)^{l+1}$, respectively. Since the kaon mass is very close to the three-pion mass, higher angular momentum are suppressed due to the centrifugal barrier, and we will consider only the values $l = 0$ and $l = 1$.

The symmetry properties of each isospin state with respect to the exchange of any two pions among the three are obtained by writing each state in terms of the various isospin configurations and of Clebsch–Gordan coefficients [6]. As summarized in Table 1, the $I = 0$ and $I = 3$ states are, respectively, antisymmetric and symmetric. There are two $I = 1$ states, one of which is symmetric. The other $I = 1$ state and the $I = 2$ state show a so-called mixed symmetry: they are symmetric and antisymmetric, respectively, only with respect to the exchange of the charged pions. In all cases a full symmetrization is obtained by an appropriate choice of the space wave functions which multiply the isospin states.

Total isospin I	Isospin state symmetry	CP eigenvalue
0	antisymmetric	$+1$
1	symmetric, mixed	-1
2	mixed	$+1$
3	symmetric	-1

Table 1: The isospin states of the $\pi^+\pi^-\pi^0$ system.

As the total angular momentum is zero, the space wave functions can be written in general as linear combinations of terms of the form [6]

$$\Phi_{k,m,n} = q_1^{2k} q_2^{2m} q_3^{2n} f_{k,m,n}(q_1^2 + q_2^2 + q_3^2)$$

where q_i are the moduli of the pion three-momenta $\vec{q}_i$ in the kaon rest frame. The indices k, m, n can take any integer value (the lowest possible values being preferred because of the small pion momenta) and $f_{k,m,n}$ is a function of $q_1^2 + q_2^2 + q_3^2$. For example, the antisymmetric state $I = 0$ is symmetrized by using the lowest order antisymmetric space function

$$\Phi = [q_1^4(q_2^2 - q_3^2) + q_2^4(q_3^2 - q_1^2) + q_3^4(q_1^2 - q_2^2)]f(q_1^2 + q_2^2 + q_3^2),$$

which shows that the $I = 0$ component is strongly suppressed by kinematics. The $I = 3$ component is instead suppressed by the $\Delta I = 1/2$ rule. The complete decomposition of the neutral-kaon decay amplitudes in terms of isospin and pion momenta can be found in Ref. [5]. More commonly, the Dalitz variables X and Y are used instead of the pion momenta for describing these amplitudes.

A further decomposition concerns the initial states K^0 and $\overline{\mathrm{K}}^0$. The corresponding decay amplitudes to a $\pi^+\pi^-\pi^0$ state with given angular momentum l and isospin I are defined as

$$A_{l,I} = a_{l,I}e^{i\delta_I} \quad \text{and} \quad \overline{A}_{l,I} = (-1)^{l+1}a^*_{l,I}e^{i\delta_I},$$

where $a_{l,I}$ describes the part of the decay amplitude coming from the weak interaction and δ_I is the rescattering phase due to the strong interaction between the final-state pions (owing to the small phase space available δ_I is expected to be small). The $\mathrm{K_L}$ and $\mathrm{K_S}$ amplitudes are then given by

$$\begin{array}{rcl} A^L_{l,I} & = & \frac{1}{\sqrt{2}}[(1+\varepsilon_{\mathrm{L}})a_{l,I} - (-1)^{l+1}(1-\varepsilon_{\mathrm{L}})a^*_{l,I}]e^{i\delta_I} \\ A^S_{l,I} & = & \frac{1}{\sqrt{2}}[(1+\varepsilon_{\mathrm{S}})a_{l,I} + (-1)^{l+1}(1-\varepsilon_{\mathrm{S}})a^*_{l,I}]e^{i\delta_I}, \end{array} \tag{1}$$

where ε_{S} and ε_{L} are the CP-violation parameters in the $\overline{\mathrm{K}}^0$–K^0 mixing. They are defined as $\varepsilon_{\mathrm{L}} = \varepsilon - \delta$ and $\varepsilon_{\mathrm{S}} = \varepsilon + \delta$. In the $\overline{\mathrm{K}}^0$–K^0 mixing ε describes T-violation and δ a possible non-conservation of CPT invariance [3]. If CPT invariance holds, $\varepsilon_{\mathrm{L}} = \varepsilon_{\mathrm{S}} = \varepsilon$.

By using Eqs. (1) and the Bose statistics symmetry requirements one can develop the $\mathrm{K_S}$ and $\mathrm{K_L}$ decay amplitudes as a function of I and of the Dalitz variables X and Y [5–12]. Considering up to quadratic terms in X and Y and neglecting direct CP violation, we obtain:

$$\begin{array}{rcl} A_{\mathrm{S}}^{3\pi(\mathrm{CP}=-1)}(X,Y) & \approx & \varepsilon_{\mathrm{S}} A_{\mathrm{L}}^{3\pi(\mathrm{CP}=-1)}(X,Y) \\ A_{\mathrm{S}}^{3\pi(\mathrm{CP}=+1)}(X,Y) & \approx & \gamma X(1+i\delta_2) - \xi_{XY}XY \\ A_{\mathrm{L}}^{3\pi(\mathrm{CP}=-1)}(X,Y) & \approx & \alpha(1+i\delta_1) - \beta Y(1+i\delta_{1M}) + \xi(Y^2 - \frac{1}{3}X^2) + \zeta(Y^2 + \frac{1}{3}X^2) \\ A_{\mathrm{L}}^{3\pi(\mathrm{CP}=+1)}(X,Y) & \approx & \varepsilon_{\mathrm{L}} A_{\mathrm{S}}^{3\pi(\mathrm{CP}=+1)}(X,Y). \end{array} \tag{2}$$

All amplitude components are related to the isospin amplitudes $a_{0,1}$ and $a_{1,2}$ of Eqs. (1) and have equal weak phases (no direct CP violation). The quantities δ_1 and δ_{1M} are rescattering phases for $I = 1$ states [7]. The rescattering phase for $I = 2$ states is δ_2. Angular momenta > 1 and final state interactions contribute to the amplitudes ξ, ξ_{XY} and ζ. These second order terms are small and their rescattering phases (which are also expected to be small) are neglected [12].

The isospin amplitudes α, β, γ, ξ, ξ_{XY} and ζ have been determined by a fit to all known neutral- and charged-kaon decay rates [7, 11] and also estimated by fits to data using Chiral Perturbation Theory (ChPT) at next-to-leading order [11, 12]. In these calculations both $\Delta I = 1/2$ and $\Delta I = 3/2$ transitions were taken into account, while the rescattering phases and their kinematical dependence were only considered in [12]. The values obtained are summarized in Table 2.

	K experiments [11]	ChPT $\mathcal{O}(p^4)$ [11]	ChPT $\mathcal{O}(p^4)$ [12]
α	$+84.3 \pm 0.6$	$+84.2$	
β	-28.1 ± 0.5	-28.1	
ζ	-0.05 ± 0.2	-0.6	
ξ	-1.3 ± 0.5	-1.4	
γ	$+2.6 \pm 0.3$	$+2.9$	
ξ_{XY}	-0.3 ± 0.7	-0.1	
δ_1	–	–	0.13
δ_{1M}	–	–	0.41
δ_2	–	–	0.047

Table 2: Expected values of the neutral-kaon amplitude components appearing in Eqs. (2). They result from fits to all known charged and neutral-kaon decay rates using either Eqs. (2 (left) or Chiral Perturbation Theory (ChPT) calculations (center and right).

The isospin amplitudes also enter the energy dependence of the Dalitz distribution for $\mathrm{K_L} \to \pi^+\pi^-\pi^0$ which is usually parametrized as

$$|\mathrm{A_L^{3\pi}}(X,Y)|^2 \propto 1 + gY + hY^2 + jX + kX^2 + fXY. \tag{3}$$

The so-called slope parameters g, h, j, k, and f are expressed in terms of the isospin amplitudes of Eqs. (2) as

$$g = -2\frac{\beta}{\alpha} \qquad h = 2\frac{\zeta+\xi}{\alpha} + \left(\frac{\beta}{\alpha}\right)^2 \qquad k = \frac{2}{3}\frac{\zeta-\xi}{\alpha} \tag{4}$$

$$j = 2\mathrm{Re}(\varepsilon_\mathrm{L})\frac{\gamma}{\alpha} \qquad f = 2\mathrm{Re}(\varepsilon_\mathrm{L})\frac{\gamma\beta}{\alpha^2}\,.$$

The expected and measured values for the slope parameters are given in Table 3. We note that a non-zero value of the slope parameters j and f would indicate CP violation in $\mathrm{K_L} \to \pi^+\pi^-\pi^0$ decays.

	K experiments [11]	ChPT $\mathcal{O}(p^4)$ [11, 12]	PDG'96 [13]
g	0.67 ± 0.01	0.67	0.670 ± 0.014
h	0.08 ± 0.01	0.06	0.079 ± 0.007
j	–	1.1×10^{-4}	0.0011 ± 0.0008
k	0.01 ± 0.04	0.006	0.0098 ± 0.0018
f	–	3.7×10^{-5}	–

Table 3: The slope parameters of $\mathrm{K_L} \to \pi^+\pi^-\pi^0$ decays. The values quoted in the first two columns were obtained from the values of the kaon decay amplitudes given in Table 2, by using Eqs. (4) and by setting $\mathrm{Re}(\varepsilon_\mathrm{L}) = \delta_l/2$ where δ_l is the charge asymmetry measured in semileptonic decays [13].

2.3 The CP-conserving and the CP-violating parameters

The $\mathrm{K_L}$ decay amplitude $A_\mathrm{L}^{3\pi(\mathrm{CP}=-1)}(X,Y)$ interferes with both the CP-conserving $\mathrm{K_S}$ decay amplitude $A_\mathrm{S}^{3\pi(\mathrm{CP}=+1)}(X,Y)$ and the CP-violating $\mathrm{K_S}$ decay amplitude $A_\mathrm{S}^{3\pi(\mathrm{CP}=-1)}(X,Y)$.

The former interference term, antisymmetric in X, is observed by separating the events with $X > 0$ and $X < 0$ and by measuring the CP-conserving parameter λ defined as

$$\lambda = \frac{\int_{Y_{\rm min}}^{Y_{\rm max}} \int_0^{X_{\rm lim}(Y)} A_{\rm L}^{*\ 3\pi({\rm CP}=-1)}(X,Y) A_{\rm S}^{3\pi({\rm CP}=+1)}(X,Y) {\rm d}X{\rm d}Y}{\int_{Y_{\rm min}}^{Y_{\rm max}} \int_0^{X_{\rm lim}(Y)} |A_{\rm L}^{3\pi({\rm CP}=-1)}(X,Y)|^2 {\rm d}X{\rm d}Y}. \tag{5}$$

This contribution vanishes when the data are integrated over the whole phase space, allowing the observation of the latter interference term through the measurement of the CP-violating parameter η_{+-0} given by

$$\eta_{+-0} = \frac{\int_{Y_{\rm min}}^{Y_{\rm max}} \int_{-X_{\rm lim}(Y)}^{+X_{\rm lim}(Y)} A_{\rm L}^{*\ 3\pi({\rm CP}=-1)}(X,Y) A_{\rm S}^{3\pi({\rm CP}=-1)}(X,Y) {\rm d}X{\rm d}Y}{\int_{Y_{\rm min}}^{Y_{\rm max}} \int_{-X_{\rm lim}(Y)}^{+X_{\rm lim}(Y)} |A_{\rm L}^{3\pi({\rm CP}=-1)}(X,Y)|^2 {\rm d}X{\rm d}Y}. \tag{6}$$

By using the parametrizations of Eqs. (2), and by neglecting second-order terms in the rescattering phase differences and second order terms proportional to $\beta\xi_{XY}$, $\gamma\xi$, $\gamma\zeta$, $\xi\xi_{XY}$ and $\zeta\xi_{XY}$, we deduce

$$\begin{aligned} \eta_{+-0} &= \varepsilon_{\rm S} \\ {\rm Re}(\lambda) &= \frac{\gamma(\alpha I_{1,0} - \beta I_{1,1}) - \alpha\xi_{XY} I_{1,1}}{\alpha^2 I_{0,0} - 2\alpha\beta I_{0,1} + \beta^2 I_{0,2}} \qquad (7) \\ {\rm Im}(\lambda) &= \frac{\gamma(\alpha(\delta_2-\delta_1) I_{1,0} - \beta(\delta_2 - \delta_{1{\rm M}}) I_{1,1}) + \alpha\xi_{XY}\delta_1 I_{1,1}}{\alpha^2 I_{0,0} - 2\alpha\beta I_{0,1} + \beta^2 I_{0,2}}\,. \qquad (8) \end{aligned}$$

The coefficients

$$I_{n,m} = \int_{Y_{\rm min}}^{Y_{\rm max}} \int_0^{X_{\rm lim}(Y)} X^n Y^m {\rm d}X{\rm d}Y$$

are given in Table 4. The parameter λ describing the interference between the $\rm K_S$ and $\rm K_L$ CP-allowed decay amplitudes, is expected to be almost real. An imaginary part could exist because of the final-state rescattering phases or a possible direct CP-violation contribution; both however are small. With the values of Table 2, we obtain for the real and imaginary parts of λ the values summarized in Table 5.

n	m	$I_{n,m}$	n	m	$I_{n,m}$	n	m	$I_{n,m}$
0	0	5.0372 ± 0.0044	1	0	4.9960 ± 0.0066	2	0	6.8879 ± 0.0121
0	1	0.5016 ± 0.0005	1	1	0.3169 ± 0.0004	2	1	0.2713 ± 0.0003
0	2	2.4358 ± 0.0042	1	2	1.9063 ± 0.0042	2	2	2.1687 ± 0.0057

Table 4: The values of the integrals $I_{n,m}$. The quoted errors are due to the uncertainties in the masses of $\rm K^0$, $\pi^\pm$ and π^0.

	K experiments [11]	ChPT $\mathcal{O}(p^4)$ [11]	ChPT $\mathcal{O}(p^4)$ [12]
${\rm Re}(\lambda)$	0.028 ± 0.003	0.031	$+0.031$
${\rm Im}(\lambda)$	–	–	-0.006

Table 5: The values for the real and imaginary parts of the CP-conserving parameter λ, as obtained from the neutral-kaon decay amplitudes given in Table 2 using Eqs. (7) and (8).

The parameter η_{+-0} measures CP violation for $\rm K_S \to \pi^+\pi^-\pi^0$. This violation is expected to be as large as CP violation for $\rm K_L \to \pi^+\pi^-$, and $\eta_{+-0} \approx \eta_{+-}$.

3 Experimental method

The CPLEAR experimental approach to the determination of η_{+-0}, λ, γ and ξ_{XY} is based on the measurement of time-dependent decay-rate asymmetries between initially tagged K^0 and $\overline{\mathrm{K}}^0$. This method allows for small systematic errors since the detector efficiency, the geometrical acceptance and the background are almost the same for K^0 and $\overline{\mathrm{K}}^0$, and thus cancel in the experimental asymmetries. Moreover, the measurement of the interference between $\mathrm{K_L}$ and $\mathrm{K_S}$ through the decay rate asymmetries allows the determination of the CP-conserving and CP-violating parameters without any theoretical assumptions on the decay amplitudes.

The measurement of the slope parameters is more conventional since it uses the Dalitz distribution of $\mathrm{K_L} \to \pi^+\pi^-\pi^0$ decays corrected by the experimental acceptance.

3.1 Decay-rate asymmetries to extract η_{+-0} and λ

The time-dependent decay rates $R_{+-0}(X,Y,\tau)$ and $\overline{R}_{+-0}(X,Y,\tau)$ for initial K^0 and $\overline{\mathrm{K}}^0$ decaying at a proper time τ to a $\pi^+\pi^-\pi^0$ state with Dalitz variables X and Y are given to first order in $\mathrm{K_S} \to \pi^+\pi^-\pi^0$ decay amplitude:

$$\begin{aligned}\frac{R_{+-0}(X,Y,\tau)}{\overline{R}_{+-0}(X,Y,\tau)} \;\propto\; & [1 \mp 2\mathrm{Re}(\varepsilon_\mathrm{S})]\,|A_\mathrm{L}^{+-0}(X,Y)|^2\,\exp(-\Gamma_\mathrm{L}\tau) \\ & \pm\{\mathrm{Re}[A_\mathrm{S}^{+-0}(X,Y)A_\mathrm{L}^{+-0}(X,Y)^*]\,\cos(\Delta m\,\tau) \\ & -\,\mathrm{Im}[A_\mathrm{S}^{+-0}(X,Y)A_\mathrm{L}^{+-0}(X,Y)^*]\,\sin(\Delta m\,\tau)\}\,\exp[-(\Gamma_\mathrm{S}+\Gamma_\mathrm{L})\tau/2]\,,\end{aligned}$$

where Δm is the $\mathrm{K_L}$–$\mathrm{K_S}$ mass difference, and Γ_L (Γ_S) is the decay width of the $\mathrm{K_L}$ ($\mathrm{K_S}$). The integration over the Dalitz plot between the Y boundaries and over $X > 0$ or $X < 0$ leads to the integrated decay rates $R_+(\tau), \overline{R}_+(\tau)$ or $R_-(\tau), \overline{R}_-(\tau)$, respectively:

$$\begin{aligned}\frac{R_+(\tau)}{\overline{R}_+(\tau)} \;\propto\; & [1 \mp 2\mathrm{Re}(\varepsilon_\mathrm{S})]\,\exp(-\Gamma_\mathrm{L}\tau) \\ & \pm 2\,[\mathrm{Re}(\eta_{+-0}+\lambda)\cos(\Delta m\,\tau) - \mathrm{Im}(\eta_{+-0}+\lambda)\sin(\Delta m\,\tau)]\,\exp[-(\Gamma_\mathrm{S}+\Gamma_\mathrm{L})\tau/2],\end{aligned}$$

$$\begin{aligned}\frac{R_-(\tau)}{\overline{R}_-(\tau)} \;\propto\; & [1 \mp 2\mathrm{Re}(\varepsilon_\mathrm{S})]\,\exp(-\Gamma_\mathrm{L}\tau) \\ & \pm 2\,[\mathrm{Re}(\eta_{+-0}-\lambda)\cos(\Delta m\,\tau) - \mathrm{Im}(\eta_{+-0}-\lambda)\sin(\Delta m\,\tau)]\,\exp[-(\Gamma_\mathrm{S}+\Gamma_\mathrm{L})\tau/2].\end{aligned}$$

The η_{+-0} contribution to the $\mathrm{K_L}$–$\mathrm{K_S}$ interference term appearing in these rates is isolated by forming the decay-rate asymmetry

$$\begin{aligned}A_{+-0}(\tau) &= \frac{[\overline{R}_+(\tau)+\overline{R}_-(\tau)]-[R_+(\tau)+R_-(\tau)]}{[\overline{R}_+(\tau)+\overline{R}_-(\tau)]+[R_+(\tau)+R_-(\tau)]} \\ &= 2\,\mathrm{Re}(\varepsilon_\mathrm{S}) \\ &\quad -2\,[\mathrm{Re}(\eta_{+-0})\,\cos(\Delta m\,\tau) - \mathrm{Im}(\eta_{+-0})\,\sin(\Delta m\,\tau)]\,\exp[-(\Gamma_\mathrm{S}-\Gamma_\mathrm{L})\tau/2].\end{aligned} \tag{9}$$

The measurement of this time-dependent asymmetry allows the determination of the CP-violating parameter η_{+-0}. Otherwise, the two asymmetries obtained by separating the rates for $X > 0$ and $X < 0$,

$$\begin{aligned}A_\pm(\tau) &= \frac{\overline{R}_\pm(\tau)-R_\pm(\tau)}{\overline{R}_\pm(\tau)+R_\pm(\tau)} \\ &= 2\,\mathrm{Re}(\varepsilon_\mathrm{S}) \\ &\quad -2\,[\mathrm{Re}\,(\eta_{+-0}\pm\lambda)\cos(\Delta m\,\tau) - \mathrm{Im}\,(\eta_{+-0}\pm\lambda)\sin(\Delta m\,\tau)]\exp[-(\Gamma_\mathrm{S}-\Gamma_\mathrm{L})\tau/2]\,,\end{aligned} \tag{10}$$

are used to determine the CP-conserving parameter λ.

The expected CP-violating and CP-conserving asymmetries are plotted in Figs. 1 and 2, respectively, as a function of the proper time measured in units of τ_S ($\tau_S = 1/\Gamma_S$). They show that the maximum sensitivity on the real and imaginary parts of the CP parameters is obtained at short decay time. Moreover, the asymmetry related to the CP-conserving amplitude is at least one order of magnitude higher than the one related to CP violation.

3.2 Decay-rate asymmetry to extract γ and ξ_{XY}

The same method can be used to directly extract the isospin components γ and ξ_{XY} of the $\mathrm{K_S} \to \pi^+\pi^-\pi^0$ amplitude. This determination, however, relies on the parametrization of the neutral-kaon decay amplitudes given in Eqs. (2). In each point of the Dalitz plot, we define the asymmetry

$$\begin{aligned} A_\xi(X,Y,\tau) &= \frac{[\overline{R}_-(X,Y,\tau) + R_+(X,Y,\tau)\,] - [\overline{R}_+(X,Y,\tau) + R_-(X,Y,\tau)\,]}{[\overline{R}_-(X,Y,\tau) + R_+(X,Y,\tau)\,] + [\overline{R}_+(X,Y,\tau) + R_-(X,Y,\tau)\,]} \\ &= 2\,|X|\frac{\gamma - \xi_{XY}Y}{\alpha - \beta Y}\,\cos(\Delta m\tau)\,\exp[-(\Gamma_\mathrm{S} - \Gamma_\mathrm{L})\tau/2], \end{aligned} \tag{11}$$

where the rescattering phases and second-order terms in X and Y are neglected. This asymmetry is then used to extract simultaneously the two isospin amplitudes γ and ξ_{XY}, by fixing the $\mathrm{K_L}$ decay amplitudes α and β to the experimental values given in Table 2.

3.3 Extraction of the $\mathrm{K_S}$ branching ratio

Although λ is determined without any theoretical inputs, the determination of the corresponding branching ratio of the CP-conserving $\mathrm{K_S} \to \pi^+\pi^-\pi^0$ requires the theoretical parametrization of the neutral-kaon decay amplitudes. The branching ratio of the CP-conserving $\mathrm{K_S}$ decay is defined as

$$\mathrm{BR}(\mathrm{K_S} \to \pi^+\pi^-\pi^0) = \frac{\Gamma_\mathrm{L}}{\Gamma_\mathrm{S}}\,\mathrm{BR}(\mathrm{K_L} \to \pi^+\pi^-\pi^0)\frac{\Gamma_\mathrm{S}^{3\pi}}{\Gamma_\mathrm{L}^{3\pi}}. \tag{12}$$

Here $\Gamma_\mathrm{S}^{3\pi}$ and $\Gamma_\mathrm{L}^{3\pi}$ are the partial decay widths for $\mathrm{K_S}$ and $\mathrm{K_L}$ decaying to $\pi^+\pi^-\pi^0$. Their ratio can be expressed as a function of the amplitudes α, β and γ in Eq. (2):

$$\frac{\Gamma_\mathrm{S}^{3\pi}}{\Gamma_\mathrm{L}^{3\pi}} = \frac{\int_{Y_\mathrm{min}}^{Y_\mathrm{max}}\int_{-X_\mathrm{lim}(Y)}^{+X_\mathrm{lim}(Y)} |A_\mathrm{S}^{3\pi(\mathrm{CP}=+1)}(X,Y)|^2 \mathrm{d}X\,\mathrm{d}Y}{\int_{Y_\mathrm{min}}^{Y_\mathrm{max}}\int_{-X_\mathrm{lim}(Y)}^{+X_\mathrm{lim}(Y)} |A_\mathrm{L}^{3\pi(\mathrm{CP}=-1)}(X,Y)|^2 \mathrm{d}X\,\mathrm{d}Y} = \gamma^2 \times \frac{I_{2,0}}{\alpha^2 I_{0,0} - 2\alpha\beta I_{0,1} + \beta^2 I_{0,2}}, \tag{13}$$

if we neglect direct CP violation and the amplitude ξ_{XY}. By combining Eq. (13) with Eqs. (7) and (12), we obtain

$$\mathrm{BR}(\mathrm{K_S} \to \pi^+\pi^-\pi^0) = \frac{\Gamma_\mathrm{L}}{\Gamma_\mathrm{S}} \times \mathrm{BR}(\mathrm{K_L} \to \pi^+\pi^-\pi^0) \times \mathrm{Re}(\lambda)^2 \times \frac{I_{2,0}(\alpha^2 I_{0,0} - 2\alpha\beta I_{0,1} + \beta^2 I_{0,2})}{(\alpha I_{1,0} - \beta I_{1,1})^2}.$$

By taking the world average value for $\mathrm{BR}(\mathrm{K_L} \to \pi^+\pi^-\pi^0)$ [13], and the experimental values for α and β given in Table 2, we obtain the following numerical relation between the desired branching ratio and $\mathrm{Re}(\lambda)$:

$$\mathrm{BR}(\mathrm{K_S} \to \pi^+\pi^-\pi^0) = \mathrm{Re}(\lambda)^2 \times (3.24 \pm 0.06) \times 10^{-4}. \tag{14}$$

4 The CPLEAR experiment

In the CPLEAR experiment, initial K^0 and $\overline{\mathrm{K}}^0$ are produced in about 4×10^{-3} of the antiproton–proton annihilations through the reactions

$$\overline{\mathrm{p}}\mathrm{p}\ \text{(at rest)}\ \rightarrow \mathrm{K}^-\pi^+\mathrm{K}^0\ \text{ and }\ \overline{\mathrm{p}}\mathrm{p}\ \text{(at rest)}\ \rightarrow \mathrm{K}^+\pi^-\overline{\mathrm{K}}^0,$$

where the conservation of strangeness in strong interaction implies that a $\overline{\mathrm{K}}^0$ is accompanied by a K^+ and a K^0 by a K^-. Thus for the above class of events (golden events) the identification of the charged kaon and the sign of its electric charge tags the strangeness of the neutral kaon at the time of production.

The CPLEAR detector [14], shown in Fig. 3, determines the strangeness of each initial neutral kaon and identifies its decay products. It has a cylindrical geometry and is mounted inside a solenoid of 3.6 m length and 1 m radius, which produces a magnetic field of 0.44 T parallel to the antiproton beam. At the centre of the detector, antiprotons with a momentum of 200 MeV/*c* are brought to rest and annihilate in a target of gaseous hydrogen at a rate of 1 MHz. For data recorded from 1992 up to 1994, the target was spherical with a radius of 7 cm and a pressure of 16 bar. During the 1994 data-taking, it was replaced by a cylindrical one with a radius of 1.1 cm at a pressure of 27 bar.

The identification of the charged kaon is performed by using a threshold Cherenkov counter sandwiched between two layers of scintillator. The Cherenkov radiator, liquid FC72, was chosen to separate efficiently charged kaons from charged pions. In the momentum range of the experiment, most pions generate Cherenkov light while the kaon momenta are below the threshold of light emission. In addition, the scintillators allow particle identification by $\mathrm{d}E/\mathrm{d}x$ and time-of-flight. They also provide fast identification of the charged particles to the trigger system.

The sign of the charge and the momentum of the charged particles are determined by the curvature of the track, measured by two proportional chambers, six drift chambers and two layers of streamer tubes. Target and tracking-chamber materials are minimized ($\approx 10^{-2} X_0$ and $\approx 5 \times 10^{-3}$ interaction length) in order to reduce multiple scattering and regeneration effects.

Photons are detected in an electromagnetic calorimeter composed of eighteen layers of lead converters and tubes working in a high-gain mode. Each of these layers is equipped with two layers of pickup strips, allowing a three-dimensional reconstruction of electromagnetic showers.

To cope with the high rate and select the neutral kaons among the multipionic annihilations, a multilevel trigger was used. It is based on the recognition of the associated $\mathrm{K}^\pm\pi^\mp$ pair at the annihilation vertex. It uses dedicated hardwired processors which reconstruct the kinematics of the event and identify the charged kaon in about 6 μs. In 1995, a cylindrical proportional chamber with a radius of 1.5 cm was added around the new target. This chamber, being very close to the annihilation vertex, was used by the first stage of the trigger to reject more efficiently the annihilation background.

For the $\pi^+\pi^-\pi^0$ final state, the data-taking started in 1992, when the calorimeter and the trigger were fully operational, and finished at the end of 1995. During this period, about 8×10^{12} antiproton–proton annihilations were collected, corresponding to about 4×10^9 events on tape.

5 Event selection and corrections

The selection of neutral kaons decaying into $\pi^+\pi^-\pi^0$ is performed by a set of topological cuts, constrained fits and particle-identification criteria. The remaining background is then estimated from the difference between data and simulated $\pi^+\pi^-\pi^0$ events properly normalized.

5.1 Topological filter

The selected events contain four charged-particle tracks, with zero total charge, and one or more electromagnetic showers in the calorimeter, which are well separated from any charged track. The latter requirement considerably reduces the background from $\mathrm{p\overline{p}}$ annihilations into $\mathrm{K^+K^-\pi^+\pi^-}$ as well as $\pi^+\pi^-$ and semileptonic decays of neutral kaons.

The $\mathrm{p\overline{p}}$ annihilation vertex is reconstructed from the charged-kaon candidate and a pion of opposite electric charge coming from the centre of the detector and thus defined as primary particles. This vertex is required to be well within the target volume. The neutral kaon decay vertex is reconstructed from the remaining π^+ and π^- tracks defined as secondary particles. The distance between the two vertices in the transverse plane is required to be greater than 1.2 cm.

The opening angle of the secondary pions has to be larger than 8° in order to remove $\mathrm{e^+e^-}$ pairs from γ conversions or π^0 Dalitz decays, and smaller than 172° in order to remove events with particles back-scattered from the detector's outer components.

At the output of the topological filter we cut on the invariant mass of the secondary particles $\pi^+\pi^-\pi^0$. The charged-pion momenta are given by the track-fit procedure while the π^0 momentum is defined as the total missing momentum in the $\mathrm{p\overline{p}}$ annihilation. The $\pi^+\pi^-\pi^0$ invariant mass has to be lower than 600 MeV/c^2 to further reject neutral-kaon decays to $\pi^+\pi^-$ and semileptonic final states.

5.2 Kinematically constrained fits

In order to further remove the background originating from $\mathrm{p\overline{p}}$ annihilations and neutral-kaon decays to other channels, events are then selected using kinematically constrained fits which also permit to improve the decay-time resolution of the selected sample. The constraints applied to satisfy the kinematics of the process $\mathrm{p\overline{p}}$(at rest) $\rightarrow \mathrm{K^-\pi^+K^0}$ with $\mathrm{K^0} \rightarrow \pi^+\pi^-\pi^0$, or its charge conjugate (c.c.), are the following:

- conservation of total energy and momentum with the constraints that the missing mass at the primary vertex is the mass of the neutral kaon, and the total missing mass is the π^0 mass;
- collinearity of the neutral kaon momentum vector and the vector connecting the primary vertex and decay vertex in the transverse plane.

Events are kept if the kinematical hypotheses are satisfied by only one track combination with a probability larger than 5%. In addition, the primary $\mathrm{K^\pm\pi^\mp}$ pair of the selected events has to be the primary $\mathrm{K^\pm\pi^\mp}$ chosen by the trigger algorithms of the hardware processors.

At this stage, the selected sample is compared to the distribution for simulated $\pi^+\pi^-\pi^0$ and semileptonic neutral-kaon decay events, as shown in Fig. 4. The contribution from neutral kaons decaying into semileptonic final states is found to be strongly suppressed at short decay times. There the decay particles, crossing the proportional chambers, have a better momentum resolution, resulting in a more efficient rejection by the constrained fits. A background, not associated with semileptonic events, is also clearly seen below 4 τ_S. This fact justifies our choice to normalize the simulated data to real data above 6 τ_S where only semileptonic events contribute to background.

We conclude that at this stage the data sample is dominantly composed of $\pi^+\pi^-\pi^0$ decays of neutral kaons with a 4% contamination of long decay-time background coming from semileptonic decays of neutral kaons, and an 8% contamination of other, short decay-time, background. This type of background may originate from $\mathrm{K_S}$ decays and $\mathrm{\overline{p}p}$ annihilation processes other than golden. Its suppression is discussed in detail in Section 5.3.

5.3 Background suppression using particle identification criteria

By simulation of neutral-kaon decays to $\pi^+\pi^-$ it was proved that, mainly owing to the effectiveness of the constrained fits, the background resulting from $\mathrm{K_S} \to \pi^+\pi^-$ decays is reduced to a negligible amount. The same holds for many other annihilation channels such as multi-pion final states, whose contribution is at most 0.002%. We estimate that at short decay times, the remaining background contributions are the following:

(a) $\mathrm{p\overline{p}} \to \mathrm{K^+\pi^-\overline{K}^0}$ (or c.c.) events with a $\mathrm{K_S}$ decaying to $\pi^0\pi^0$, followed by a π^0 Dalitz decay to $\mathrm{e^+e^-\gamma}$;

(b) $\mathrm{p\overline{p}} \to \mathrm{K^+K^-\pi^+\pi^-}$ events passing the selection criteria because of a badly reconstructed track;

(c) $\mathrm{p\overline{p}} \to \pi^0\mathrm{K^+\pi^-\overline{K}^0}$ (or c.c.) events, where a $\mathrm{K_S}$ decays into $\pi^+\pi^-$ and the primary charged pion is taken as a secondary pion and vice versa, even though the vertex resolution in the transverse plane is ≈ 1.5 mm.

These backgrounds are further reduced by kinematical cuts and particle-identification criteria chosen by comparing real data and simulated $\mathrm{K^0, \overline{K}^0} \to \pi^+\pi^-\pi^0$ decays.

The Dalitz decay events of type (a) are almost fully eliminated by removing events where the invariant mass of the secondary particles, computed with the $\mathrm{e^+e^-}$ hypothesis, is small and the measured time-of-flight is not compatible with a $\pi^+\pi^-$ pair.

Events of type (b) are reduced by discarding events where the four- or three-track vertex-fit probability is high and the total missing momentum is low. In addition, the time-of-flight information of the charged particles is used to confirm the primary $\mathrm{K}\pi$ and secondary $\pi\pi$ hypotheses.

Events of type (c) are rejected if the cross-combination fulfils invariant-mass and vertex alignment constraints consistent with the $\mathrm{p\overline{p}} \to \pi^0\mathrm{K^+\pi^-\overline{K}^0}$ ($\mathrm{K_S} \to \pi^+\pi^-$) or c.c. hypothesis. These cuts are only applied to events with at least three tracks coming from the centre of the detector. The rejection of this background is illustrated in Fig. 5, showing the $\pi^+\pi^-$ invariant mass of the cross-combination for real data with a decay time smaller than 2 τ_S before and after applying the cuts.

The addition of the new proportional chamber close to the centre of the detector (see Section 4) allowed an improvement of the selection criteria for the 1995 data sample, by requiring a hit in this chamber for the primary $\mathrm{K^\pm\pi^\mp}$ tracks and no hit associated with the secondary particles of the neutral-kaon decay. This condition allowed the release of the cuts described above in order to reject $\mathrm{p\overline{p}} \to \mathrm{K^+K^-\pi^+\pi^-}$ and $\mathrm{p\overline{p}} \to \pi^0\mathrm{K^+\pi^-\overline{K}^0}$ (or c.c.) background, and led to a substantial increase (about 30%) in the signal acceptance at short decay times.

However, the new amount of material around the annihilation region had also enhanced the production of $\Lambda(1115) \to \mathrm{p}\pi^-$ through $\mathrm{\overline{K}^0}$ or $\mathrm{K^-}$ interactions with nuclei ($\mathrm{K^-}$ originated from $\mathrm{K^+K^-\pi^+\pi^-}$ background). These processes only contaminate the $\mathrm{\overline{K}^0}$ data set, thus simulating a CP-violation asymmetry. The Λ(1115) signal is located well below 1.25 τ_S, with a maximum at 0.75 τ_S. It amounts to $\approx$ 20% of the previous short decay-time background. Figure 6 shows the Λ(1115) signal in the invariant-mass distribution of the secondary particles with the $\mathrm{p}\pi^-$ hypothesis, for $\mathrm{\overline{K}^0}$ events with a decay-time lower than 0.75 τ_S. The Λ(1115) background is reduced by a factor of two by using the time-of-flight information to identify the proton. Since the remaining amount of Λ(1115) background is at the limit of our sensitivity, the induced $\mathrm{\overline{K}^0}$–$\mathrm{K^0}$ asymmetry is treated as a source of systematic error.

With these criteria, the final data set contains a total of 508 000 events with a decay time between 0.25 and 19.75 τ_S. The $\pi^+\pi^-\pi^0$ invariant-mass distribution of the selected events is shown in Fig. 7, together with the distribution for simulated $\pi^+\pi^-\pi^0$ and semileptonic neutral-kaon decay events. The corresponding decay-time distributions which eventually give the back-

ground/signal ratio are discussed in Section 5.4.

5.4 Remaining background in the final data set

Figure 8 shows the real and simulated decay-time distributions of the selected data sample. The simulated distribution, given by the sum of neutral-kaon decays to $\pi^+\pi^-\pi^0$ and to $\pi l \nu_l$ weighted with the corresponding $\mathrm{K_L}$ branching ratios, is normalized to the real data for decay times above 6 τ_S, where semileptonic decays are the only source of background. The normalization factor is obtained by fitting a constant to the ratio of these two decay-time distributions.

The excess of data up to 1.25 τ_S represents our short decay-time background whose origins have been discussed in the previous section. The excess of simulated events around 2.5 τ_S can be associated to an imperfect simulation of the proportional-chamber hit resolution for a neutral-kaon decay vertex close to the wire plane (at a radius of 10 cm). Since the chamber response had been calibrated with single tracks, for the purpose of this analysis we performed a fine tuning of the two-hit resolution and so matched the simulated decay-radius distribution to the measured one.

It is important to note that the improvement in the chamber simulation does not affect the evaluation of the short decay-time background, because the latter originates at a radius (< 4 cm) much smaller than the proportional chamber radius. The additional error introduced on this background, owing to the tuning, is about 10%, which is negligible compared with the overall uncertainty discussed in Section 6.1.2.

The total-background fraction of the events $\zeta_\mathrm{B}(\tau)$, in the time interval between 0.25 τ_S and 19.75 τ_S, is defined as the relative difference between the data and the simulated $\pi^+\pi^-\pi^0$ events. Figure 9 shows the total-background fraction as a function of the decay time, and also the line, parametrized as the sum of a linear and an exponential term, which is fitted to the data points. The linear part describes the semileptonic contribution while the exponential part accounts for the short decay-time background below 1.25 τ_S.

When fitting the asymmetries to data (see Section 6), the total-background fraction is taken into account by using this parametrization of $\zeta_\mathrm{B}(\tau)$:

$$\begin{aligned}\zeta_\mathrm{B}(\tau) \;=\; & \exp\{-[0.2 \pm 0.6\ (\mathrm{stat.})] - [4.1 \pm 1.3\ (\mathrm{stat.})] \times \Gamma_\mathrm{S}\tau\} \\ & -[0.008 \pm 0.004\ (\mathrm{stat.})] + [0.0062 \pm 0.0004\ (\mathrm{stat.})] \times \Gamma_\mathrm{S}\tau].\end{aligned}$$

The total semileptonic component is found to be 4.15% while the total short decay-time background is 0.16%.

5.5 Decay-rate corrections

Before constructing the experimental asymmetries corresponding to Eqs. (9), (10) and (11), three corrections were applied to the data.

The first takes into account the dependence of the tagging efficiency of $\overline{\mathrm{K}}^0$ relative to K^0 on the charged-kaon and pion momenta. The tagging efficiencies of $\overline{\mathrm{K}}^0$ and K^0 are equal to the detection efficiencies, $\epsilon(\mathrm{K}^+,\pi^-)$ and $\epsilon(\mathrm{K}^-,\pi^+)$ respectively, of the associated primary $\mathrm{K}\pi$ pair. They are not identical owing to the different strong interaction cross-sections of K^+ and K^-, and of π^+ and π^-, in the detector. These effects induce an average difference at the level of 12% between the K^0 and $\overline{\mathrm{K}}^0$ tagging efficiencies. In addition, the momentum dependence of the cross-section introduces a difference in the decay-time distributions at a level of 1%, since the momentum distributions are related to the decay time. This correlation arises from the finite decay volume and the decay-radius dependent acceptance. To correct for this distortion, a

normalization factor $\xi_{\rm N}(\vec{p_{\rm K}},\vec{p_\pi})$, defined as $\epsilon({\rm K}^+,\pi^-)/\epsilon({\rm K}^-,\pi^+)$, was measured with the $\pi^+\pi^-$ data set at short decay time, since it does not depend on the decay mode of the neutral kaon. The neutral-kaon decay-time distribution is then corrected by weighting each event with the measured detection-efficiency ratio which depends on the kinematics of the events. After this procedure, the time dependence of $\epsilon({\rm K}^0)$ and $\epsilon(\overline{\rm K}^0)$ is the same, and the overall normalization between 0.25 and 19.75 $\tau_{\rm S}$,

$$\frac{N(\overline{\rm K}^0\to\pi^+\pi^-\pi^0)}{N({\rm K}^0\to\pi^+\pi^-\pi^0)}=\frac{\int_0^{20\tau_{\rm S}}\epsilon(\overline{\rm K}^0,\tau)[\overline{R}_+(\tau)+\overline{R}_-(\tau)]{\rm d}\tau}{\int_0^{20\tau_{\rm S}}\epsilon({\rm K}^0,\tau)[R_+(\tau)+R_-(\tau)]{\rm d}\tau}=[1+4{\rm Re}(\varepsilon_{\rm S})]\times\xi_{\rm N},$$

is preserved. The mean normalization $\xi_{\rm N}$ is equal to $\langle\epsilon(\overline{\rm K}^0)\rangle/\langle\epsilon({\rm K}^0)\rangle$.

The second correction comes from the coherent regeneration which appears when neutral kaons cross our detector. Owing to the small amount of material in the central region, the expected difference in the ${\rm K}^0$ and $\overline{\rm K}^0$ decay-time distributions is up to a few per mil. To correct for this effect, each event is weighted by the ratio of the decay probability of a neutral kaon propagating in vacuum to its decay probability when it travels through the detector. This ratio is computed by using, for the forward-scattering amplitudes of ${\rm K}^0$ and $\overline{\rm K}^0$ in the momentum region of this experiment, the results of ref. [15] which agree well with the recent CPLEAR measurements [16].

The third correction takes into account the fact that the cuts removing $\pi^0{\rm K}^+\pi^-\overline{\rm K}^0$ (or c.c.) background act differently on the two secondary pions, depending on the charge of the primary kaon. This induces a fake asymmetry between the $X>0$ and $X<0$ samples, at a level of 1%, distorting the measurement of the CP-conserving parameters. Therefore, each decay rate is corrected for this effect as estimated from simulated distributions.

6 Measurement of the CP-violating and the CP-conserving parameters

The selected data set contains neutral kaons decaying into $\pi^+\pi^-\pi^0$ and some residual background. Since the amounts of ${\rm K}^0$ and $\overline{\rm K}^0$ are slightly different, the experimental decay-rate asymmetries are equal to

$$\begin{aligned}A_k^{\rm exp}(\tau) &= \frac{\overline{N}_k(\tau)-N_k(\tau)}{\overline{N}_k(\tau)+N_k(\tau)}\\ &\approx \left(\frac{\xi_{\rm N}-1}{\xi_{\rm N}+1}\right)+\frac{4\xi_{\rm N}[1-\zeta_{\rm B}(\tau)]}{(\xi_{\rm N}+1)^2}A_k(\tau),\end{aligned}\qquad(15)$$

where the subscript k refers to the Dalitz plot integration domain, $\xi_{\rm N}$ is the mean normalization factor, $\zeta_{\rm B}(\tau)$ is the parametrization of the total-background fraction as a function of the decay time. $A_{+-0}(\tau)$ is given by Eq. (9) and $A_+(\tau)$ (resp. $A_-(\tau)$) by Eq. (10). When fitting these asymmetries to the data, the CP parameters in A_k and the mean normalization factor, $\xi_{\rm N}$, are left to vary freely. In Eq. (15), the ${\rm Re}(\varepsilon_{\rm S})$ coming from A_k in Eqs. (9) and (10) is taken to be equal to ${\rm Re}(\varepsilon_{\rm L})$ and fixed to $\delta_l/2$. The world average values are used for Δm and $\Gamma_{\rm S}$ [17], δ_l and $\Gamma_{\rm L}$ [13].

6.1 Measurement of the CP-violating parameter η_{+-0}

The experimental asymmetry $A_{+-0}^{\rm exp}(\tau)$ obtained from the complete data set is shown in Fig. 10 together with the result of the fit. The fit of Eq. (9) to the data yields

$$\begin{aligned}{\rm Re}(\eta_{+-0}) &= (-2\pm7\ ({\rm stat.}))\times10^{-3}\\ {\rm Im}(\eta_{+-0}) &= (-2\pm9\ ({\rm stat.}))\times10^{-3}\\ \xi_{\rm N} &= 1.116\pm0.004\ ({\rm stat.})\end{aligned}$$

with a $\chi^2/\mathrm{d.o.f.} = 0.86$ and with the following statistical correlation coefficients:

	$\mathrm{Re}(\eta_{+-0})$	$\mathrm{Im}(\eta_{+-0})$	ξ_{N}
$\mathrm{Re}(\eta_{+-0})$	1		
$\mathrm{Im}(\eta_{+-0})$	$+0.68$	1	
ξ_{N}	-0.21	-0.51	1

Table 6 summarizes the systematic errors which affect the determination of η_{+-0}. They mainly come from differences in the background content between the K^0 and $\overline{\mathrm{K}}^0$ data sets which are not described by the background parametrization. To isolate the background component at short decay times, K^0 and $\overline{\mathrm{K}}^0$ data were added together. This eliminates, to first order, any CP-conserving or CP-violating effects coming from $\mathrm{K_S}$ decays. The $\zeta_{\mathrm{B}}(\tau)$ parametrization cannot be determined separately for K^0 and $\overline{\mathrm{K}}^0$.

Source of systematic error	$\mathrm{Re}(\eta_{+-0})\,[10^{-3}]$	$\mathrm{Im}(\eta_{+-0})\,[10^{-3}]$
Pionic and kaonic background – amount and normalization	$\begin{pmatrix} +1.5 \\ -0.7 \end{pmatrix}$	$\begin{pmatrix} +0.7 \\ -0.2 \end{pmatrix}$
$\Lambda(1115)$ background	+4.1	+1.9
CP-conserving $\mathrm{K_S}$ decay amplitude	–0.1	–
Decay-time dependence of normalization *	± 0.2	± 0.4
Decay-time resolution	± 0.2	± 0.2
Regeneration	< 0.1	< 0.1
Δm, Γ_{S}, $\Gamma_{\mathrm{L}}$and $\mathrm{Re}(\varepsilon_{\mathrm{S}})$	–	–

* Error determination limited by statistics.

Table 6: Summary of the systematic errors on the real and imaginary parts of η_{+-0}

.

6.1.1 Method for evaluating the systematic uncertainties

The systematic errors due to uncertainties on the knowledge of the short decay-time background, the finite binning and the decay-time resolution are estimated by using a simplified simulation of our data sets. The decay-time of signal and background events is generated according to their decay-time distributions:

(a) The decay-time distributions of signal events with positive and negative X are constructed from the phenomenological decay rates of K^0 and $\overline{\mathrm{K}}^0$, calculated with the expected values of $\mathrm{Re}(\eta_{+-0})$, $\mathrm{Im}(\eta_{+-0})$, $\mathrm{Re}(\lambda)$ and $\mathrm{Im}(\lambda)$ and multiplied by the acceptance of $\pi^+\pi^-\pi^0$ events. The acceptance is parametrized according to a set of Monte Carlo events fully simulated.

(b) The decay-time distribution of background events is obtained separately for the semileptonic and short decay-time background. The semileptonic contribution is generated according to the phenomenological decay rates multiplied by the corresponding acceptances. The short decay-time contribution is obtained by subtracting the semileptonic distribution from the total background given by $\zeta_{\mathrm{B}}(\tau)$ times the simulated rate of the signal.

The decay time of each generated event is then smeared according to the decay time resolution determined with the full simulation. From each set of simulated decay rates, containing $\approx 5 \times 10^5$ events, CP asymmetries are formed and fitted in order to determine the values of η_{+-0}.

This procedure is repeated 2000 times to minimize the effect of statistical fluctuations. The systematic error of η_{+-0} is then estimated by the difference between the average of the fitted values and the expected one.

This procedure is applied by varying the different parameters which are possible sources of systematic errors within their estimated accuracy. The resulting systematic errors are given in Table 6. For a more detailed discussion see below.

6.1.2 Discussion of systematic uncertainties

- *Amount and normalization of short decay-time background*
  The amount and the shape of the short decay-time background are estimated by comparing the decay-time distribution of real data and of simulated $\pi^+\pi^-\pi^0$ and $\pi l\nu_l$ events. In order to evaluate the uncertainty on the amount of short decay-time background, we use the decay-radius distribution and we compare the simulated distribution normalized to the data at various decay-radius intervals. The first interval between 4 and 7 cm is far away from the position of the first proportional chamber at 10 cm and thus free from any effect resulting from an acceptance distortion (see Section 5.4). The second region was chosen between the second proportional chamber at 13 cm and the first drift chamber at 25 cm. The amount of short decay-time background evaluated beween 0 and 4 cm depends on the value used for the normalization to the data and ranges between 0.16% and 0.36%.

  Since the charged-kaon momentum distribution of this background is different from the signal, the $\overline{\mathrm{K}}^0/\mathrm{K}^0$ normalization of the background at short decay time may also be different from the signal. We have then analysed samples of $\mathrm{K}^+\mathrm{K}^-\pi^+\pi^-$ and of $\pi^0\mathrm{K}^0\pi^+\mathrm{K}^-$ (or c.c.) events, defined as being rejected by the associated cuts. The $\overline{\mathrm{K}}^0/\mathrm{K}^0$ normalization factor measured for the first class of events is 1.146 ± 0.019, and 1.108 ± 0.023 for the second. The systematic error of η_{+-0} was estimated by using in our simplified simulation the maximum amount for the background at short decay time (0.36%), and for the $\overline{\mathrm{K}}^0/\mathrm{K}^0$ normalization factor the central values given above $\pm$ one standard deviation.
- *The Λ(1115) background*
  The fraction of $\Lambda(1115) \to \mathrm{p}\pi^-$ events (only contained in the $\overline{\mathrm{K}}^0$ data set) was estimated by constructing the invariant-mass distribution of the secondary particles with the $\mathrm{p}\pi^-$ hypothesis and counting the excess of real data events over simulated $\overline{\mathrm{K}}^0 \to \pi^+\pi^-\pi^0$ decays in the mass window between 1105 and 1125 MeV/c^2 (Fig. 6), and turned out to be (0.013 ± 0.006)%. The decay-time distribution was obtained by counting the excess of events as a function of the decay-time when the time-of-flight cut was relaxed. The systematic error of η_{+-0} was estimated by introducing in the simplified simulation a $\Lambda(1115)$ background, with its decay time distribution, for an amount of 0.019%, and only for $\overline{\mathrm{K}}^0$ decay rate.
- *CP-conserving $\mathrm{K_S}$ decay amplitude*
  The CP-conserving $\mathrm{K_S}$ amplitude does not cancel in the CP-violating asymmetry $A_{+-0}(\tau)$ if there is any difference in the detector acceptance $\epsilon(X,Y)$ for the phase-space regions $X > 0$ and $X < 0$. In that case, the interference between the CP-conserving $\mathrm{K_S}$ and $\mathrm{K_L}$ amplitudes integrated over the whole phase space does not cancel and contributes to $\mathrm{Re}(\eta_{+-0})$ through the additional term

$$T_{\mathrm{CP}} = \frac{\int_{Y_{\min}}^{Y_{\max}} \int_{-X_{\lim}(Y)}^{+X_{\lim}(Y)} \epsilon(X,Y) A_{\mathrm{L}}^{*\ 3\pi(\mathrm{CP}=-1)}(X,Y) A_{\mathrm{S}}^{3\pi(\mathrm{CP}=+1)}(X,Y) \mathrm{d}X\,\mathrm{d}Y}{\int_{Y_{\min}}^{Y_{\max}} \int_{-X_{\lim}(Y)}^{+X_{\lim}(Y)} \epsilon(X,Y) |A_{\mathrm{L}}^{3\pi(\mathrm{CP}=-1)}(X,Y)|^2 \mathrm{d}X\,\mathrm{d}Y}.$$

  This term is evaluated directly from our data, taking into account all the acceptance distortions. We obtained $T_{\mathrm{CP}} = (-0.7 \pm 0.4) \times 10^{-4}$. The systematic error of η_{+-0} is given

by the $T_{\rm CP}$ central value minus one standard deviation.

- *Decay-time dependence of normalization*
  The error introduced by the statistical uncertainties in the $\overline{\rm K}^0/{\rm K}^0$ normalization correction was taken into account. The data were also corrected for any time dependence of the normalization. A search for any residual effect due to different trigger topologies was carried out and found to lead to a small error.
- *Decay-time resolution*
  The decay-time resolution varies from ≈ 0.05 up to 0.2 $\tau_{\rm S}$ in our decay-time range. The systematic effects due to the finite decay-time resolution, bin size, and the lower limit of the decay-time interval used in fitting the asymmetry, are correlated. The resulting error was thus determined at once by using our simplified simulation.
- *Regeneration*
  The effect of neutral-kaon regeneration in the detector material is expected to be negligible. The asymmetry is maximal at short decay time, and in that region near the centre of the detector the amount of material was very small. The uncertainty of the correction was found to be less than a few 10^{-5} when changing the regeneration amplitudes within the uncertainties of the values extrapolated from higher energy data ($\pm 13\%$ for the modulus and $\pm 9^\circ$ for the phase [18]).
- Δm *,* $\Gamma_{\rm S}$ *,* $\Gamma_{\rm L}$ *and* $\mathrm{Re}(\varepsilon_{\rm S})$
  The experimental uncertainties on the values of Δm [17], $\Gamma_{\rm S}$, $\Gamma_{\rm L}$ and $\mathrm{Re}(\varepsilon_{\rm S})$ [13] used in the fit have negligible impact on the results. We note that the value of η_{+-0} obtained from the fit is insensitive to to a possible difference between $\mathrm{Re}(\varepsilon_{\rm S})$ and $\delta_l/2$, within the known limits on $\mathrm{Re}(\delta)$ related to CPT invariance [19]. In our analysis a value of $\mathrm{Re}(\delta) < 3\times 10^{-4}$ would shift $\mathrm{Re}(\eta_{+-0})$ by $< 0.6 \times 10^{-4}$ and $\mathrm{Im}(\eta_{+-0})$ by $< 1.5 \times 10^{-4}$.

6.1.3 *Final results on the CP-violating parameter* η_{+-0}

Our final result on η_{+-0}, shown in Fig. 11, is

$$\mathrm{Re}(\eta_{+-0}) = \left(-2 \pm 7\,(\text{stat.}) \;\; {}^{+4}_{-1} \;\; (\text{syst.})\right) \times 10^{-3}$$
$$\mathrm{Im}(\eta_{+-0}) = \left(-2 \pm 9\,(\text{stat.}) \;\; {}^{+2}_{-1} \;\; (\text{syst.})\right) \times 10^{-3}.$$

Assuming no correlation between the systematic errors, we obtain $|\eta_{+-0}| < 0.017$ at the 90% confidence level.

To cross-check the internal consistency of our data set, we performed the same analysis after splitting the selected sample according to the data-taking period. The mean value of η_{+-0} of these individual measurements is then determined by using a χ^2 technique which is minimized in the (Re, Im, $\xi_{\rm N}$) space taking into account the covariance matrix of each individual measurement. A $\chi^2/\mathrm{d.o.f}$ greater than one would indicate that the statistical error and the statistical correlation are not large enough to explain the observed dispersion. The result of this analysis is given in Fig. 12. The mean values obtained are much the same as the results of the standard analysis, showing the consistency of our data. The resulting $\chi^2/\mathrm{d.o.f.} = 0.96$ indicates that the dispersion of the measurements around the mean value is dominated by statistical fluctuations.

The values obtained in this work constitute the most precise determination of the real and imaginary parts of η_{+-0}. Compared to the published values of Barmin et al. [20] and Zou et al. (only $\mathrm{Im}(\eta_{+-0})$) [21], our errors are smaller by more than one order of magnitude and by a

factor of four, respectively. However, our sensitivity on the CP-violating parameter is still one order of magnitude away from the expected CP-violation effect.

6.2 Measurement of the CP-conserving parameter λ

For the measurement of the CP-conserving parameter λ, the data set is split into two parts according to the sign of the Dalitz variable X. The experimental asymmetries $A_+^{\rm exp}(\tau)$ and $A_-^{\rm exp}(\tau)$ are formed on the corresponding samples. Their time dependences, given by Eq. (15), are fitted to the data in two steps. Firstly, a simultaneous six-parameter fit of the functions $A_+^{\rm exp}(\tau)$ and $A_-^{\rm exp}(\tau)$ to the relevant data set gives the following results:

$$\begin{aligned}
{\rm Re}(\eta_{+-0}) &= [-2 \pm 7\ ({\rm stat.})] \times 10^{-3} \\
{\rm Im}(\eta_{+-0}) &= [-2 \pm 9\ ({\rm stat.})] \times 10^{-3} \\
\\
{\rm Re}(\lambda) &= [+27 \pm 7\ ({\rm stat.})] \times 10^{-3} \\
{\rm Im}(\lambda) &= [-12 \pm 9\ ({\rm stat.})] \times 10^{-3} \\
\\
\xi_{\rm N}^{X<0} &= 1.118 \pm 0.005\ ({\rm stat.}) \\
\xi_{\rm N}^{X>0} &= 1.114 \pm 0.005\ ({\rm stat.})
\end{aligned}$$

with a $\chi^2/{\rm d.o.f.} = 0.88$ and with the following statistical correlation matrix:

	${\rm Re}(\eta_{+-0})$	${\rm Im}(\eta_{+-0})$	$\xi_{\rm N}^{X>0}$	$\xi_{\rm N}^{X<0}$	${\rm Re}(\lambda)$	${\rm Im}(\lambda)$
${\rm Re}(\eta_{+-0})$	1					
${\rm Im}(\eta_{+-0})$	+0.677	1				
$\xi_{\rm N}^{X>0}$	−0.149	−0.364	1			
$\xi_{\rm N}^{X<0}$	−0.147	−0.362	0	1		
${\rm Re}(\lambda)$	+0.008	+0.003	−0.149	+0.147	1	
${\rm Im}(\lambda)$	+0.003	+0.004	−0.364	+0.362	0.677	1

The results on ${\rm Re}(\eta_{+-0})$ and ${\rm Im}(\eta_{+-0})$ are identical to those obtained by fitting the experimental asymmetry integrated over the whole Dalitz plot. Since there is almost no correlation between the components of η_{+-0} and λ, the statistical accuracy on the mean normalization can be improved without any implicit assumption on direct CP violation or CPT invariance by fixing η_{+-0} to the known value of η_{+-} [13]. In addition, since $\xi_{\rm N}^{X>0}$ and $\xi_{\rm N}^{X<0}$ are statistically compatible, we can assume $\xi_{\rm N}^{X>0} = \xi_{\rm N}^{X<0} = \xi_{\rm N}$. Therefore, in the second step, a simultaneous fit of the asymmetries $A_+^{\rm exp}(\tau)$ and $A_-^{\rm exp}(\tau)$ is performed by varying freely λ and $\xi_{\rm N}$ and by fixing η_{+-} to the world average value [13]. It is shown in Fig. 13 with the result of the fit. The fit yields

$$\begin{aligned}
{\rm Re}(\lambda) &= [+28 \pm 7\ ({\rm stat.})] \times 10^{-3} \\
{\rm Im}(\lambda) &= [-10 \pm 8\ ({\rm stat.})] \times 10^{-3} \\
\xi_{\rm N} &= 1.116 \pm 0.003\ ({\rm stat.})
\end{aligned}$$

with a $\chi^2/{\rm d.o.f.} = 0.85$ and with the following statistical correlation coefficients:

	${\rm Re}(\lambda)$	${\rm Im}(\lambda)$	$\xi_{\rm N}$
${\rm Re}(\lambda)$	1		
${\rm Im}(\lambda)$	+0.68	1	
$\xi_{\rm N}$	0	0	1

Source of systematic error	$\mathrm{Re}(\lambda)[10^{-3}]$	$\mathrm{Im}(\lambda)[10^{-3}]$
Pionic and kaonic background – amount and Xasymmetry	$\begin{pmatrix} +1.3 \\ -1.4 \end{pmatrix}$	$\begin{pmatrix} +0.5 \\ -0.3 \end{pmatrix}$
$\Lambda(1115)$ background – amount and Xasymmetry	$\begin{pmatrix} +0.7 \\ -2.3 \end{pmatrix}$	$\begin{pmatrix} +0.2 \\ -0.8 \end{pmatrix}$
Decay-time dependence of normalization*	± 0.2	± 0.2
Decay-time resolution	+1.1	+0.7
Regeneration	< 0.1	< 0.1
Δm and Γ_{S}	± 0.1	$\begin{pmatrix} +0.1 \\ -0.2 \end{pmatrix}$
Acceptance	± 2.0	± 1.8

* Error determination limited by statistics.

Table 7: Summary of the systematic errors on the real and imaginary parts of λ.

Since the measured value of λ is not correlated with ξ_{N} , and thus with $\mathrm{Re}(\varepsilon_{\mathrm{S}})$, having $\mathrm{Re}(\varepsilon_{\mathrm{S}}) = \delta_l/2$ results in a λ value which is insensitive to a possible CPT violation (see also Section 6.1).

Table 7 summarizes the systematic errors which affect the determination of λ. They are largely the same as those affecting the determination of η_{+-0}. We note, however, that the sensitivity to the normalization is weak in the simultaneous fit (there is no correlation between λ and ξ_{N}) and the uncertainty on the background normalization also cancels in first order. On the other hand, the difference between the two halves, $X > 0$ and $X < 0$, of the Dalitz plot, and the difference in the background normalization lead to the dominant systematic error on λ. In the following section only systematic errors specific to the λ measurement are discussed.

6.2.1 Discussion of systematic uncertainties

- *Short decay-time background asymmetry in X*
  The normalization of the background at short decay time may be different for $X > 0$ and $X < 0$. This is the case for the $\pi^0\mathrm{K}^+\pi^-\overline{\mathrm{K}}^0$ (or c.c.) background where the interchange of the primary pion with the secondary pion introduces a systematic shift of X since the variable X is proportional to the difference $E_{\mathrm{CM}}(\pi^+) - E_{\mathrm{CM}}(\pi^-)$ and on average primary pions have a larger energy than secondary pions. The reconstructed X is thus mainly positive for K^0–tagged events and mainly negative for $\overline{\mathrm{K}}^0$–tagged events, simulating a CP-conserving asymmetry. To quantify this effect, we introduce a background normalization difference $y_B = \xi^B_{X<0} - \xi^B_{X>0}$ which is measured on the pure $\pi^0\mathrm{K}^-\pi^+\mathrm{K}^0$ (or c.c.) sample. We obtained $y_B = 0.17 \pm 0.04$. The systematic error of λ was determined by by using in our simplified simulation the maximum amount of background at short decay-time, with a normalization-factor difference given by the y_B central value $\pm$ one standard deviation.
- *Λ(1115) background asymmetry in X*
  The $\Lambda(1115) \to \mathrm{p}\pi^-$ background component may also be asymmetric in X owing to the misidentification of the proton as a pion, shifting the reconstructed X towards a negative value. These events amounting to 0.013% deviate from the symmetric case by $(10 \pm 20)\%$. The systematic error of λ was determined by introducing in the simplified simulation the maximum amount of Λ background with an X asymmetry given by the above central value $\pm$ one standard deviation.
- *Acceptance*

If the detector acceptance $\epsilon(X,Y)$ is properly folded with the right-hand part of Eq. (5), we see that the result of our measurement is

$$\lambda^{\rm exp} = \frac{\int_{Y_{\rm min}}^{Y_{\rm max}} \int_0^{+X_{\rm lim}(Y)} \epsilon(X,Y) A_{\rm L}^{*\ 3\pi({\rm CP}=-1)}(X,Y) A_{\rm S}^{3\pi({\rm CP}=+1)}(X,Y) {\rm d}X{\rm d}Y}{\int_{Y_{\rm min}}^{Y_{\rm max}} \int_0^{+X_{\rm lim}(Y)} \epsilon(X,Y) |A_{\rm L}^{3\pi({\rm CP}=-1)}(X,Y)|^2 {\rm d}X{\rm d}Y}$$

instead of λ. The difference between $\lambda^{\rm exp}$ and λ has been determined by numerical integration of simulated $\rm K^0, \overline{K}^0 \to \pi^+\pi^-\pi^0$ events, using the isospin decomposition of the $\rm K_S$ and $\rm K_L$ decay amplitudes in Eq. (2) and the expected values for α, β and γ (Table 2). The real and imaginary parts of the difference so obtained, $\Delta[{\rm Re}(\lambda)] = (+1.1 \pm 2.0) \times 10^{-3}$ and $\Delta[{\rm Im}(\lambda)] = (+0.3 \pm 1.8) \times 10^{-3}$, were considered as the systematic uncertainties of the results.

6.2.2 Final results on the CP-conserving parameter λ

Our final result on λ, also shown in Fig. 14, is

$$\begin{aligned} {\rm Re}(\lambda) &= [+28 \pm 7\,({\rm stat.}) \pm 3\,({\rm syst.})] \times 10^{-3} \\ {\rm Im}(\lambda) &= [-10 \pm 8\,({\rm stat.}) \pm 2\,({\rm syst.})] \times 10^{-3}. \end{aligned}$$

To cross-check the statistical consistency of the measurements, we repeated the analysis separately for each data-taking period. The mean values of λ, obtained by a χ^2-fit using the statistical errors and their correlations, are shown in Fig. 15 and are equal to those of the standard analysis with $\chi^2/{\rm d.o.f.} = 1.3$.

The branching ratio for the CP-conserving $\rm K_S \to \pi^+\pi^-\pi^0$ decays is calculated using Eq. (14). We obtained

$${\rm BR}({\rm K_S} \to \pi^+\pi^-\pi^0) = \left(2.5\ {}^{+1.3}_{-1.0}\ ({\rm stat.})\ {}^{+0.5}_{-0.6}\ ({\rm syst.})\right) \times 10^{-7},$$

where the systematic error also includes a contribution from the uncertainties on the $\rm K_L$ decay amplitudes.

We can also deduce a limit on the rescattering phase difference $(\delta_2 - \delta_1)$ from our measured value of ${\rm Im}(\lambda)$, using Eq. (8). In this relation, the term proportional to ξ_{XY} is dropped since its influence is negligible. By taking for the amplitudes α, β and γ the values expected by ChPT (Table 2), and by assuming an uncertainty of $\pm\pi$ on $(\delta_2 - \delta_{1M})$, we obtain at the 90% confidence level

$$-46^\circ < (\delta_2 - \delta_1) < 9^\circ.$$

This limit is dominated by the total uncertainty on ${\rm Im}(\lambda)$.

	K expts. [11]	ChPT [11]	ChPT [12]	E621 [22]	CPLEAR
${\rm Re}(\lambda)$	0.028 ± 0.003	0.031	$+0.031$	$+0.038 \pm 0.010$	$+0.028 \pm 0.008$
${\rm Im}(\lambda)$	–	–	-0.006	-0.006 ± 0.012	-0.010 ± 0.008

Table 8: The CP-conserving parameter λ as measured by CPLEAR. For comparison the values of Table 5 are also reported.

In conclusion, Table 8 shows a comparison of the values on λ obtained in this work with the values given by a phenomenological fit to all known kaon decay rates [11], ChPT [11, 12] and the best previous experiment [22]. Our result is currently the most precise determination of the CP-conserving $\rm K_S$ decay rate into $\pi^+\pi^-\pi^0$ with negligible systematic errors and is in good agreement with previous measurements.

7 Measurement of the isospin components of the $\mathrm{K_L}$ and $\mathrm{K_S}$ decay amplitudes

We determine the slope parameters of the $\mathrm{K_L}$ decay into $\pi^+\pi^-\pi^0$, which are related to the amplitude components α, β, ξ and ζ of Eq. (2). To this purpose we make use of the parametrization of the detector acceptance and of a likelihood function of the $\mathrm{K_L}$ decay rate in the (X, Y, τ) space. We also measure the interference between the $\mathrm{K_S}$ and $\mathrm{K_L}$ states as a function of the Dalitz variables X and Y, and extract the isospin components γ and ξ_{XY} of the $\mathrm{K_S}$ decay amplitudes by a maximum-likelihood fit of the time-dependent asymmetry $A_\xi(X, Y, \tau)$, Eq. (11). These measurements have all an intrinsic interest. Moreover, by comparison with those of previous experiments, they provide an overall consistency check of the control quality of our systematic errors.

7.1 Measurement of the slope parameters of the $\mathrm{K_L} \to \pi^+\pi^-\pi^0$ decays

The slope parameters defined in Eq. (3) are extracted by fitting the energy dependence of the $\mathrm{K_L} \to \pi^+\pi^-\pi^0$ events in the Dalitz plot. The Dalitz distribution is constructed from initial $\mathrm{K^0}$ and $\overline{\mathrm{K}}^0$ events in the decay-time interval between 2 τ_S and 24 τ_S so to remove the $\mathrm{K_S}$ component and the short decay-time background.

To correct for the variation of the acceptance across the Dalitz plot and the semileptonic background, the simulated distributions of $\mathrm{K_L} \to \pi^+\pi^-\pi^0, \pi\mu\nu_\mu$ and $\pi\mathrm{e}\nu_\mathrm{e}$ decays are parametrized using orthogonal polynomials in the Dalitz variables X and Y [24]. Then a function of the form of Eq. (3) multiplied by the simulation acceptance is fitted to the data.

To avoid binning problems, the maximum-likelihood technique is used. The method of simulated annealing [25, 26] is applied in order to ensure the fit convergence of the acceptance functions and of the Dalitz plot density. In addition, the $\mathrm{K^0}$ events are weighted by the mean normalization factor ξ_N to take into account the different amount of $\mathrm{K^0}$ and $\overline{\mathrm{K}}^0$.

To obtain the Dalitz-plot slope parameters, the events were split into samples corresponding to disjunct decay-time intervals of 2 τ_S width where the acceptance is assumed not to depend on the decay time. For every decay-time interval, the acceptance is determined separately. The problem of parametrizing the acceptance as a function of the decay time, in addition to X and Y, is thereby avoided. These event samples were separately fitted to obtain the slope parameters as a function of the decay time and the results then averaged with a minimum-χ^2 procedure. The results of the fit are shown in Fig. 16. We obtained for the slope parameters (all errors statistical)

$$\begin{aligned} g &= 0.682 \pm 0.004 \\ h &= (6.1 \pm 0.4) \times 10^{-2} \\ j &= (1.0 \pm 2.4) \times 10^{-3} \\ k &= (1.04 \pm 0.17) \times 10^{-2} \\ f &= (4.5 \pm 2.4) \times 10^{-3}, \end{aligned}$$

with the following correlation matrix:

	g	h	j	k	f
g	1				
h	$+0.011$	1			
j	-0.050	$+0.075$	1		
k	$+0.003$	$+0.031$	-0.017	1	
f	$+0.066$	$+0.060$	$+0.055$	$+0.005$	1

The correlations between the slope parameters are small.

Source of systematic error	$g[10^{-3}]$	$h[10^{-2}]$	$j[10^{-3}]$	$k[10^{-3}]$	$f[10^{-3}]$
Acceptance shape	± 3.8	± 1.4	± 2.8	± 2.3	± 5.6
Acceptance statistics	± 2.3	± 0.1	± 0.9	± 0.5	± 1.7
Resolution in X and Y	± 0.5	± 0.1	± 0.6	± 0.5	± 1.0
Radiative corrections	-	-	-	-	-
Normalization	-	-	-	-	-
Semileptonic background	-	-	-	-	-
Regeneration	-	-	-	-	-

Table 9: Summary of the systematic errors on the $\mathrm{K_L} \to \pi^+\pi^-\pi^0$ slope parameters.

The systematic errors are summarized in Table 9. Contrary to the determination of η_{+-0} and λ which are based on asymmetries, the determination of the slope parameters depends crucially on the knowledge of the acceptance shape. However, the systematic errors related to the short decay-time background are negligible since only data with decay times above 2 τ_{S} are used in the analysis.

- *Acceptance shape*
  The main source of systematic errors is the uncertainty in the the relative acceptance across the Dalitz plot as given by simulation. Owing to the acceptance shape varying with the decay time, the systematic error could be estimated from the dispersion of the slope parameters for different decay-time slices.
- *Acceptance statistics*
  The coefficients of the polynomials in X and Y used for the parametrization of the Dalitz-plot acceptance have errors due to the limited Monte Carlo statistics. These errors were propagated to the errors on the slope parameters.
- *Resolution in X and Y*
  To determine the error due to the resolution in X and Y, not included in the likelihood function, the simulated data were split into two samples of equal size. One of these samples was used to determine the acceptance parametrization and the other one to simulate the data. The systematic errors were evaluated by comparing the results when using the true and the reconstructed values of X and Y.
- *Radiative corrections*
  The values for the slope parameters are affected by radiative corrections [27]. We took them into account and we corrected the slope parameters by $\Delta g = -0.0008$, $\Delta h = -0.0004$, $\Delta k = +0.0002$ and $\Delta f = +0.0009$. The value of j was not affected by this correction within the quoted accuracy. The systematic errors due to uncertainties on these corrections are negligible.
- *Normalization*
  An error in the $\mathrm{K^0}$–$\overline{\mathrm{K}}^0$ normalization leads to an unequal amount of $\mathrm{K^0}$ and $\overline{\mathrm{K}}^0$ in the Dalitz distribution, introducing an additional contribution coming from the $\mathrm{K_S}$–$\mathrm{K_L}$ interference. The errors on the slope parameters were obtained by varying the normalization factor within its uncertainty. The resulting errors are negligible.
- *Background*
  In the decay time interval used for the determination of the slope parameters, only the semileptonic background is relevant. The amount of background was varied within its errors to establish the influence on the slope parameters. The effect was found to be negligible.

- *Regeneration*
  The influence of the regeneration correction was checked by repeating the analysis without this correction and comparing the results on the slope parameters. The resulting changes are negligible.

The final results on the slope parameter are

$$\begin{aligned} g &= 0.6823 \pm 0.0044\ (\mathrm{stat.}) \pm 0.0044\ (\mathrm{syst.}) \\ h &= [6.1 \pm 0.4\ (\mathrm{stat.}) \pm 1.5\ (\mathrm{syst.})] \times 10^{-2} \\ j &= [1.0 \pm 2.4\ (\mathrm{stat.}) \pm 3.0\ (\mathrm{syst.})] \times 10^{-3} \\ k &= [1.04 \pm 0.17\ (\mathrm{stat.}) \pm 0.24\ (\mathrm{syst.})] \times 10^{-2} \\ f &= [4.5 \pm 2.4\ (\mathrm{stat.}) \pm 5.9\ (\mathrm{syst.})] \times 10^{-3}. \end{aligned}$$

	K experiments [11]	ChPT $\mathcal{O}(p^4)$ [11, 12]	PDG'96 [13]	CPLEAR
g	0.67 ± 0.01	0.67	0.670 ± 0.014	0.682 ± 0.007
h	0.08 ± 0.01	0.06	0.079 ± 0.007	0.061 ± 0.015
j	–	1.1×10^{-4}	0.0011 ± 0.0008	0.001 ± 0.004
k	0.01 ± 0.04	0.006	0.0098 ± 0.0018	0.010 ± 0.003
f	–	3.7×10^{-5}	–	$(4.5 \pm 6.4) \times 10^{-3}$

Table 10: The slope parameters of the $\mathrm{K_L}$ decays into $\pi^+\pi^-\pi^0$. The values measured by CPLEAR are compared with the values reported in Table 3.

Table 10 shows the comparison of the CPLEAR results with other existing results summarized in Table 3. In general, good agreement is found, as well as an improvement in the determination of the parameter g by a factor of two.

From the observed slope parameters and the experimental value of α given in Table 2, we can deduce, using Eq. (4), the values for the $\mathrm{K_L}$ decay amplitudes β, ξ and ζ which are reported in Table 12.

7.2 Measurement of the $\mathrm{K_S}$ decay amplitudes γ and ξ_{XY}

The components γ and ξ_{XY} of the $\mathrm{K_S}$ decay amplitude were extracted from our data by fitting the experimental asymmetry

$$\begin{aligned} A_\xi^{\mathrm{exp}}(X,Y,\tau) &= \frac{[\overline{N}_-(X,Y,\tau) + N_+(X,Y,\tau)] - [\overline{N}_+(X,Y,\tau) + N_-(X,Y,\tau)]}{[\overline{N}_-(X,Y,\tau) + N_+(X,Y,\tau)] + [\overline{N}_+(X,Y,\tau) + N_-(X,Y,\tau)]} \\ &\approx [1 - \zeta_{\mathrm{B}}(X,Y,\tau)] \iint A_\xi(u,v,\tau) \times G_X(X-u) \times G_Y(Y-v)\mathrm{d}u\mathrm{d}v, \end{aligned}$$

where $\zeta_{\mathrm{B}}(X,Y,\tau)$ is the parametrization of the total-background fraction of as a function of the decay time τ and the Dalitz variables X and Y, A_ξ is the theoretical asymmetry given by Eq. (11), and the functions G_X and G_Y are Gaussian distributions describing the X and Y resolutions. Their standard deviations were determined by using simulated neutral-kaon decays at short decay time.

The amplitudes γ and ξ_{XY} entering in the calculation of A_ξ are determined by minimizing the log-likelihood function defined as [23]

$$-\frac{\ln L}{2} = \sum_{j\in S} w_j \ln[1 + A_\xi^{\mathrm{exp}}(X_j,Y_j,\tau_j)] + \sum_{j\in\overline{S}} w_j \ln[1 - A_\xi^{\mathrm{exp}}(X_j,Y_j,\tau_j)],$$

where the data set S contains K^0 events with positive X and $\overline{\mathrm{K}}^0$ events with negative X , and $\overline{S}$ contains K^0 events with negative X and $\overline{\mathrm{K}}^0$ events with positive X. In addition, w_j is a weight which takes into account the time dependence of the $\overline{\mathrm{K}}^0/\mathrm{K}^0$ tagging efficiency, the coherent regeneration and the distortion in X and Y introduced by the $\pi^0\mathrm{K}^0\pi^+\mathrm{K}^-$ (or c.c.) cuts. The latter correction was estimated from a parametrization as a function of X, Y and τ of the acceptance of these cuts. It was determined with simulated events.

When fitting this asymmetry to the data, γ and ξ_{XY} vary freely while α and β are fixed to the experimental values given in Table 2. We also used the world average values for Δm, Γ_{S} and Γ_{L} [13]. The fit yields

$$\begin{aligned} \gamma &= 3.3 \pm 0.4\ (\mathrm{stat.}) \\ \xi_{XY} &= 0.4 \pm 0.7\ (\mathrm{stat.}), \end{aligned}$$

with a correlation of 8% between the two extracted parameters.

Source of systematic error	γ	ξ_{XY}
Amount of background and background asymmetry in X	$\left(\begin{array}{c}+0.20\\-0.06\end{array}\right)$	$\left(\begin{array}{c}+0.31\\-0.05\end{array}\right)$
$\Lambda(1115)$ background and asymmetry in X	$\left(\begin{array}{c}+0.12\\-0.32\end{array}\right)$	$\left(\begin{array}{c}+0.05\\-0.28\end{array}\right)$
Decay-time resolution	+0.10	+0.01
Regeneration	–	–
Δm and Γ_{S}	± 0.01	–
α and β	± 0.03	± 0.03

Table 11: Summary of the systematic errors on γ and ξ_{XY}.

Table 11 summarizes the systematic errors which affect the determination of γ and ξ_{XY}. Their sources are identical to those for the determination of λ. The resulting systematic errors were estimated by using a simplified simulation where the neutral-kaon decay rates, the background distribution and the signal acceptance are parametrized as a function of X, Y and τ. The uncertainties associated with the acceptance cancel in this asymmetry. The effect of the experimental uncertainties on the values of α and β used in the fit are negligible.

The final results on γ and ξ_{XY} are

$$\begin{aligned} \gamma &= 3.3 \pm 0.4\ (\mathrm{stat.}) \pm 0.3\ (\mathrm{syst.}) \\ \xi_{XY} &= 0.4 \pm 0.7\ (\mathrm{stat.}) \pm 0.3\ (\mathrm{syst.}). \end{aligned}$$

By using Eq. (7), with the above values of γ and ξ_{XY} the resulting $\mathrm{Re}(\lambda)$ can be compared with the measured one obtained when $\mathrm{Im}(\lambda)$ is fixed to zero. Both determinations of $\mathrm{Re}(\lambda)$ agree within the errors, confirming our understanding of the X and Y dependence on the background.

In Table 12, we compare the results on γ and ξ_{XY} with the values given by both a phenomenological fit to all known kaon decay rates and ChPT calculations [11, 12]. Our direct measurement of γ and ξ_{XY} is in agreement with these values and has a comparable uncertainty.

8 Summary and conclusions

Using a technique which employs time-dependent decay-rate asymmetries between initially tagged $\overline{\mathrm{K}}^0$ and K^0 CPLEAR studied the neutral-kaon decays into $\pi^+\pi^-\pi^0$.
CPLEAR obtains the most accurate determination of the CP-violating parameter η_{+-0} and the

	K expts. [11]	ChPT [11]	ChPT [12]	PDG'96 [13]	CPLEAR
α	$+84.3 \pm 0.6$	$+84.2$		–	–
β	-28.1 ± 0.5	-28.1		-28.2 ± 0.6	-28.8 ± 0.3
ζ	-0.05 ± 0.2	-0.6		-0.08 ± 0.2	-0.5 ± 0.4
ξ	-1.3 ± 0.5	-1.4		-1.3 ± 0.2	-1.8 ± 0.4
γ	$+2.6 \pm 0.3$	$+2.9$		–	$+3.3 \pm 0.5$
ξ_{XY}	-0.3 ± 0.7	-0.1		–	$+0.4 \pm 0.8$
δ_1	–	–	0.13	–	–
δ_{1M}	–	–	0.41	–	–
δ_2	–	–	0.047	–	–
$\delta_2 - \delta_1$	–	–	-0.083	–	-0.33 ± 0.29

Table 12: Summary of the values of the neutral-kaon decay amplitude components appearing in Eqs. (2). For comparison we report in the first three columns the values of Table 2. The last two columns contain experimental values either (β, ζ and ξ) computed from the measured values of the slope parameters given in Table 3, using Eqs. (4) with $\alpha = +84.3 \pm 0.6$, or (γ and ξ_{XY}) directly measured by CPLEAR. The quantity $(\delta_2 - \delta_1)$ is computed from the value of $\mathrm{Im}(\lambda)$ measured by CPLEAR, using Eq. (8) and the amplitude values given by ChPT.

branching ratio of the $\mathrm{K_S}$ decay into $\pi^+\pi^-\pi^0$. The latter is in agreement with the results of a phenomenological fit of both neutral- and charged-kaon decay rates and with the prediction of Chiral Perturbation Theory.

By analysing the Dalitz-plot distributions of the sum of $\overline{\mathrm{K}}^0$ and K^0 decaying into $\pi^+\pi^-\pi^0$, CPLEAR extracts the amplitude components β, γ, ξ, ξ_{XY} and ζ contributing to the $\mathrm{K_S}$ and $\mathrm{K_L}$ decays. The observed values are in agreement with the world averages as well as with the prediction of Chiral Perturbation Theory.

Acknowledgements

We would like to thank the CERN LEAR staff as well as the technical and engineering staff of our institutes for their support and co-operation. This work was supported by the following institutions: the French CNRS/Institut National de Physique Nucléaire et de Physique des Particules, the French Commissariat à l'Energie Atomique, the Greek General Secretariat of Research and Technology, the Netherlands Foundation for Fundamental Research on Matter (FOM), the Portuguese JNICT, the Ministry of Science and Technology of the Republic of Slovenia, the Swedish Natural Science Research Council, the Swiss National Science Foundation, the UK Particle Physics and Astronomy Research Council (PPARC), and the US National Science Foundation.

References

[1] L.M. Sehgal and L. Wolfenstein, Phys. Rev. 162 (1967) 1362
B.R. Martin and E. de Rafael, Nucl. Phys. B 8 (1968) 131
E. Gabathuler and P. Pavlopoulos, Proc. Workshop on Physics at LEAR with Low Energy Cooled Antiproton, Erice, 1982, Ed. U. Gastaldi and R. Klapisch (Plenum Press, New-York, 1984) 747

[2] L. Lavoura, Mod. Phys. Lett. A 7 (1992) 1367

[3] R. Adler et al., CPLEAR Collaboration, Proc. Workshop on K Physics, Orsay, 1996, Ed. L. Iconomidou-Fayard (Editions Frontières, Gif-sur-Yvette, 1997) 307

[4] R. Adler et al., CPLEAR Collaboration, Phys. Lett. B 407 (1997) 193

[5] C. Zemach, Phys. Rev. 133 (1964) 1201

[6] W. Grimus, Fortschr. Phys. 36 (1988) 201

[7] T.J. Devlin and J.O. Dickey, Rev. Mod. Phys. 51 (1979) 237

[8] L.-F. Li and L. Wolfenstein, Phys. Rev. D 21 (1980) 178

[9] S. Fajfer and J.M Gerard, Z. Phys. C 42 (1989) 425

[10] H.-Y. Cheng, Phys. Lett. B 238 (1990) 399

[11] J. Kambor et al., Phys. Lett. B 261 (1991) 496

[12] G. D'Ambrosio et al., Phys. Rev. D 50 (1994) 5767 and ibid. D 51 (1995) 3975(E)

[13] R.M. Barnett et al., Particle Data Group, Phys. Rev. D 54 (1996) 1

[14] R. Adler et al., CPLEAR Collaboration, Nucl. Instrum. Methods A 379 (1996) 76

[15] P.H. Eberhard et al., Nucl. Instrum. Methods Phys. A 350 (1994) 144

[16] A. Angelopoulos et al., CPLEAR Collaboration, Phys. Lett. B 413 (1997) 422.

[17] R. Adler et al., CPLEAR Collaboration, Phys. Lett. B 369 (1996) 367, update with CPLEAR full statistics to be published

[18] R. Adler et al., CPLEAR Collaboration, Phys. Lett. B 363 (1995) 243

[19] CPLEAR Collaboration, CP, T and CPT violation in the neutral kaon system, Proc. HEP97, Jerusalem,1997, in print.

[20] V.V. Barmin et al., Nuovo Cimento A 85 (1985) 67

[21] Y. Zou et al., Phys. Lett. B 329 (1994) 519

[22] Y. Zou et al., Phys. Lett. B 369 (1996) 362

[23] R. Barlow and P. Hinde, Comp. Phys. Comm. 53 (1990) 325

[24] M. Weisfeld, Numerische Mathematik 1 (1959) 38

[25] M. Metropolis, J. Chem. Phys. 21 (1953) 1087

[26] S. Kirckpatrick et al., Science 220 (1983) 671

[27] A. Neveu et al., Phys. Lett. B 27 (1968) 384
R. Ferrari et al., Nuovo Cimento A 56 (1968) 582

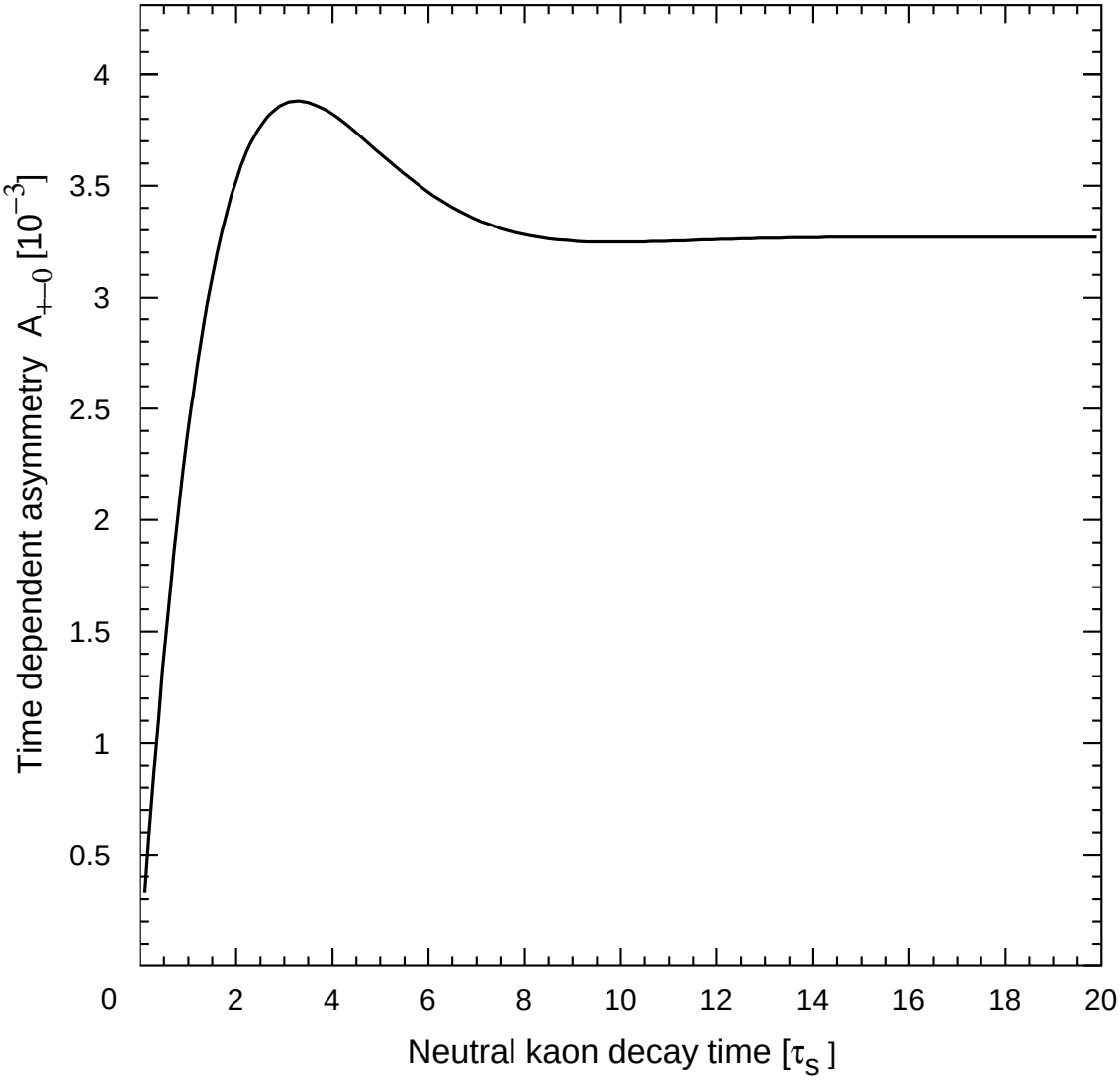

Figure 1: The expected time-dependent decay-rate asymmetry $A_{+-0}(\tau)$, Eq. (9), computed by assuming $\eta_{+-0} = \eta_{+-}$ and by taking the world average values for η_{+-}, $\Gamma_{\rm S}$, $\Gamma_{\rm L}$ and Δm [13].

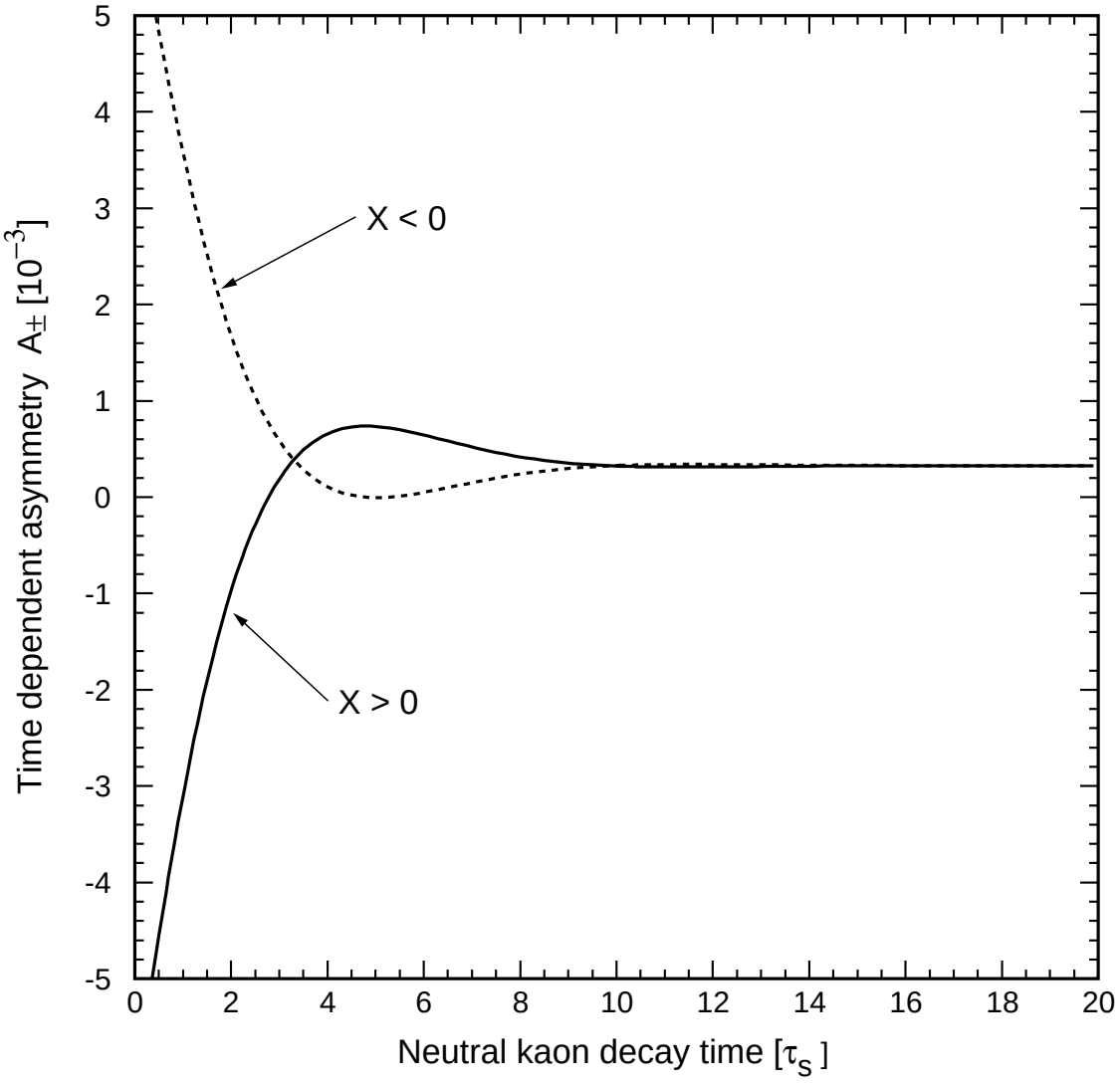

Figure 2: The expected time-dependent decay-rate asymmetries $A_+(\tau)$ for $X > 0$ and $A_-(\tau)$ for $X < 0$, Eq. (10), computed by taking $\eta_{+-0} = \eta_{+-}$, the world average values for η_{+-}, $\Gamma_{\rm S}$, $\Gamma_{\rm L}$, Δm [13] and the expected value of λ, Table 5, last column.

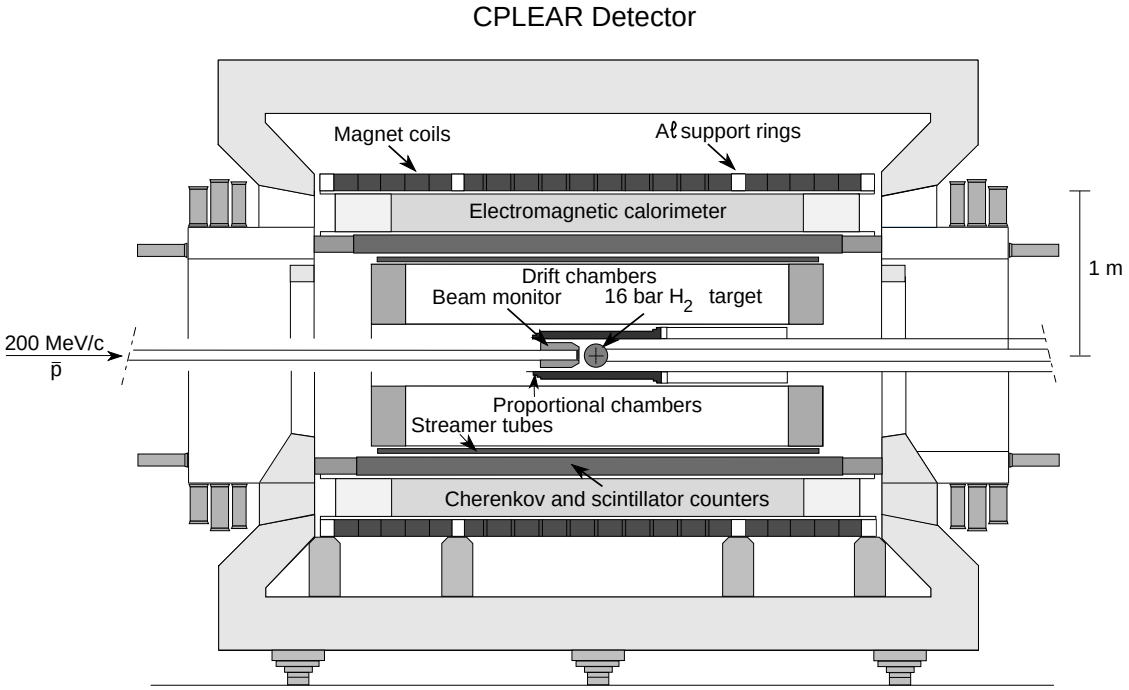

Figure 3: A longitudinal view of the CPLEAR detector up to mid 1994.

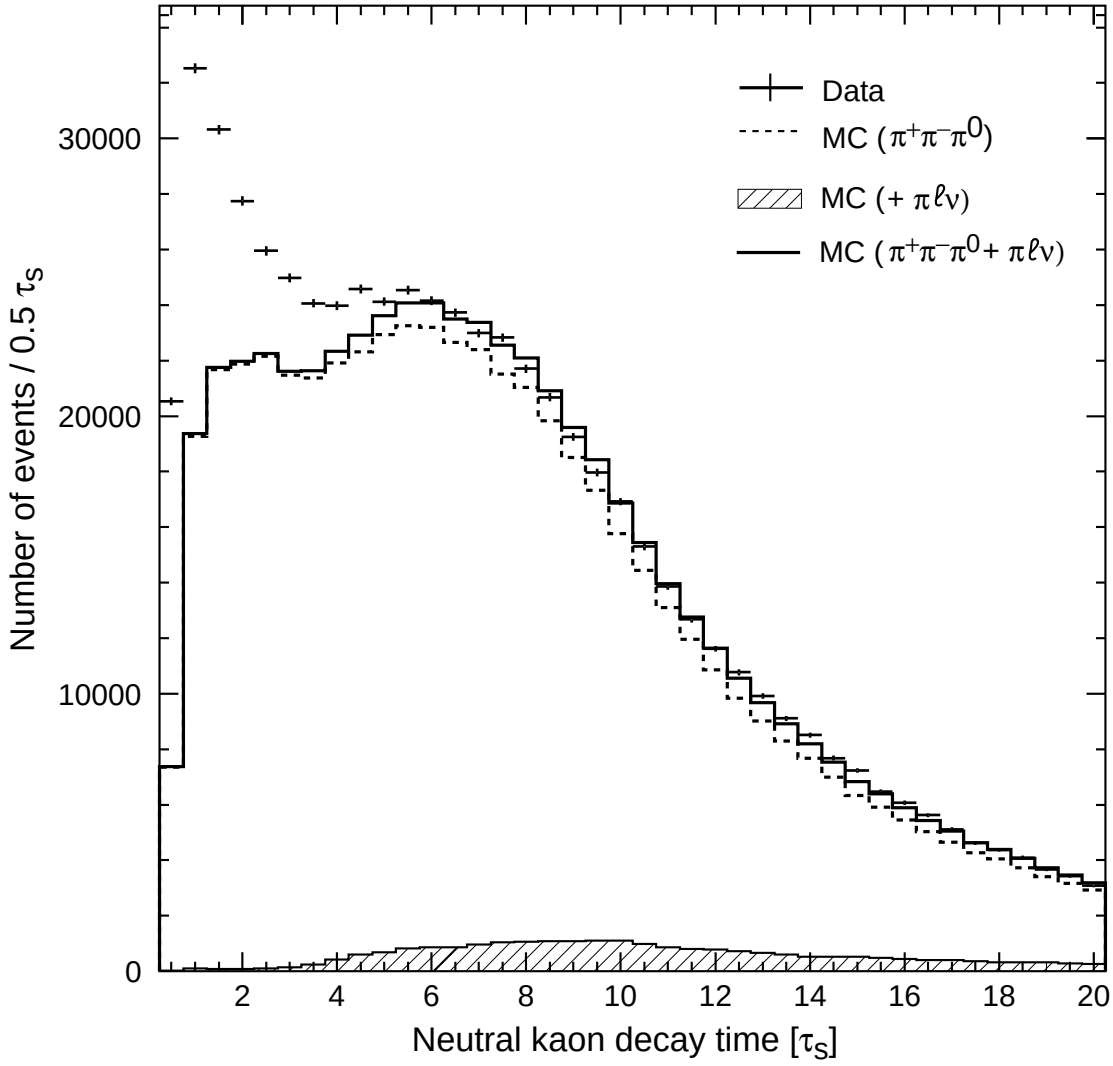

Figure 4: The decay-time distribution of the sum of initial K^0 and $\overline{\mathrm{K}}^0$ decaying into $\pi^+\pi^-\pi^0$ for real and simulated data after applying the topological filter and kinematically constrained fits. The full line shows the simulated distribution built from the sum of the $\pi^+\pi^-\pi^0$ and semileptonic decays of neutral-kaons, normalized to the real data set above 6 τ_S. The distribution of the simulated $\pi^+\pi^-\pi^0$ events is shown by the dashed line, while the background contribution from semileptonic events is given by the shaded area. The excess of real data at short decay time shows the short decay-time background at this intermediate stage of the analysis.

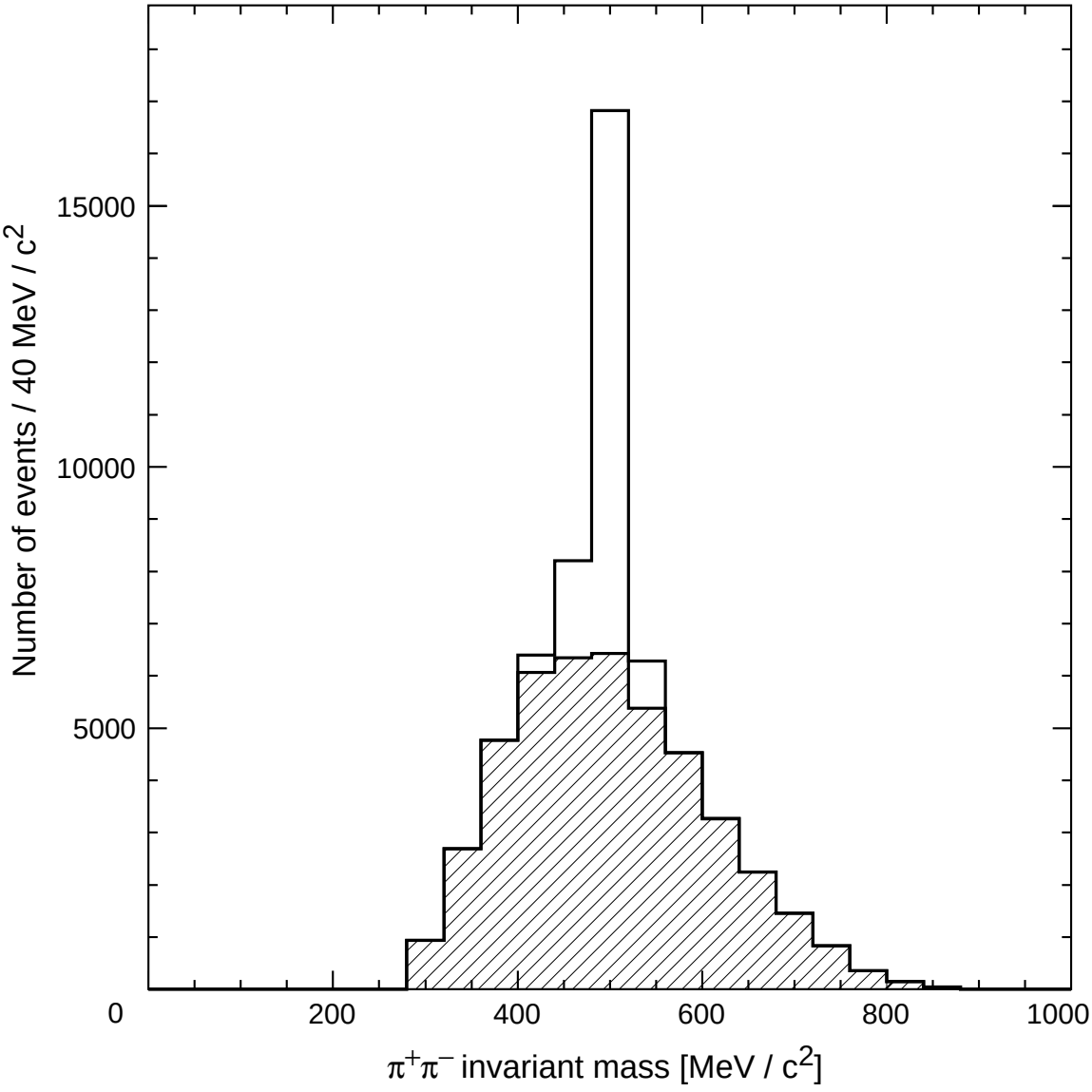

Figure 5: The invariant-mass distribution of the $\pi^+\pi^-$ cross-combination pair for real data events with a decay time smaller than 2 τ_{S} plotted before (unshaded area) and after (shaded area) applying the criteria rejecting the $\overline{\mathrm{p}}\mathrm{p} \to \pi^0\mathrm{K}^+\pi^-\overline{\mathrm{K}}^0(\mathrm{K}_{\mathrm{S}} \to \pi^+\pi^-)$ or c.c. events.

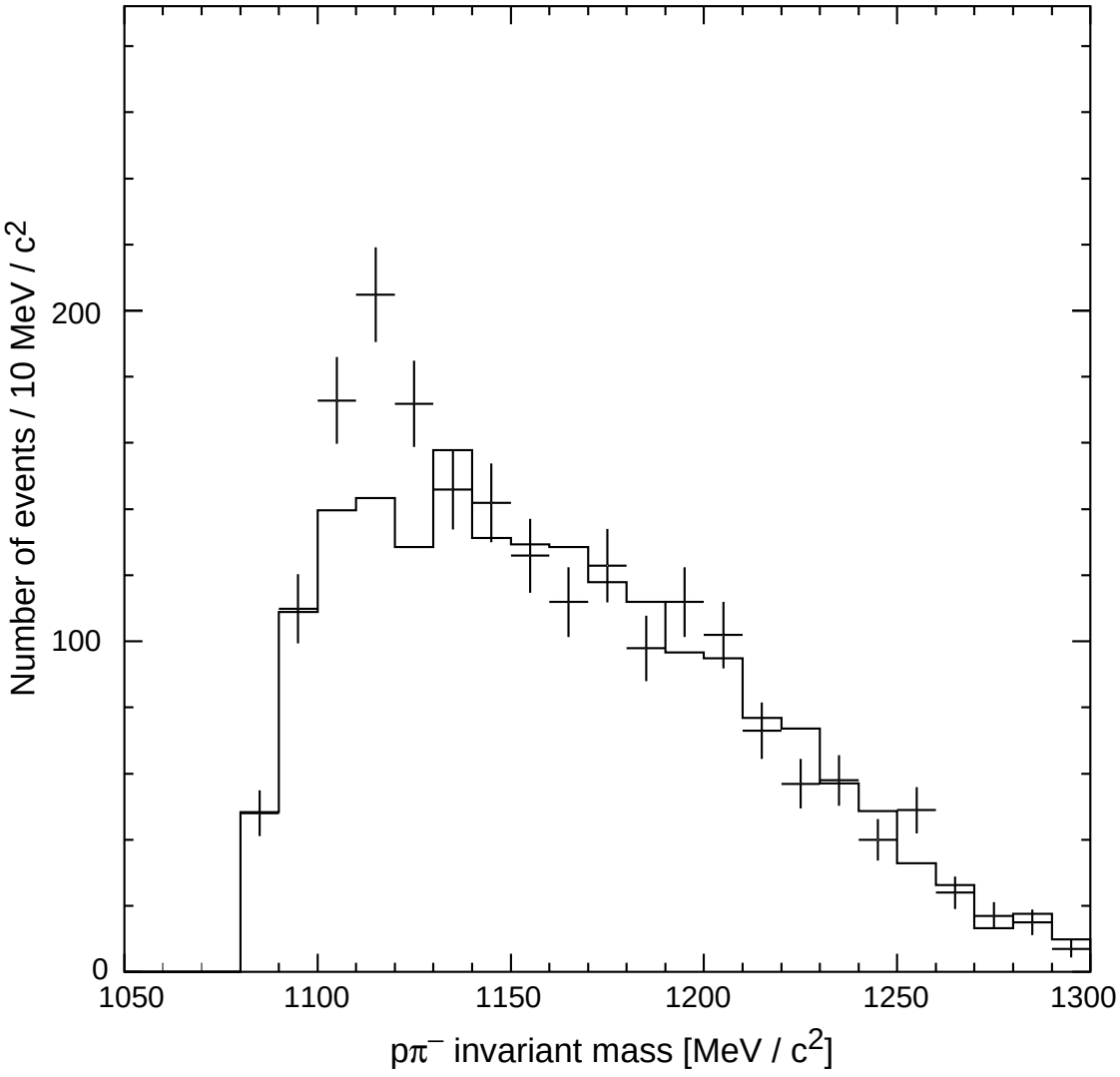

Figure 6: The invariant-mass distribution of the secondary particles with the $\mathrm{p}\pi^-$ hypothesis, for $\overline{\mathrm{K}}^0$ events with a decay-time below 0.75 τ_{S} before applying the time-of-flight cut. The excess of events appearing around 1115 MeV/c^2 shows the $\Lambda(1115)$ background component, in the 1995 data sample.

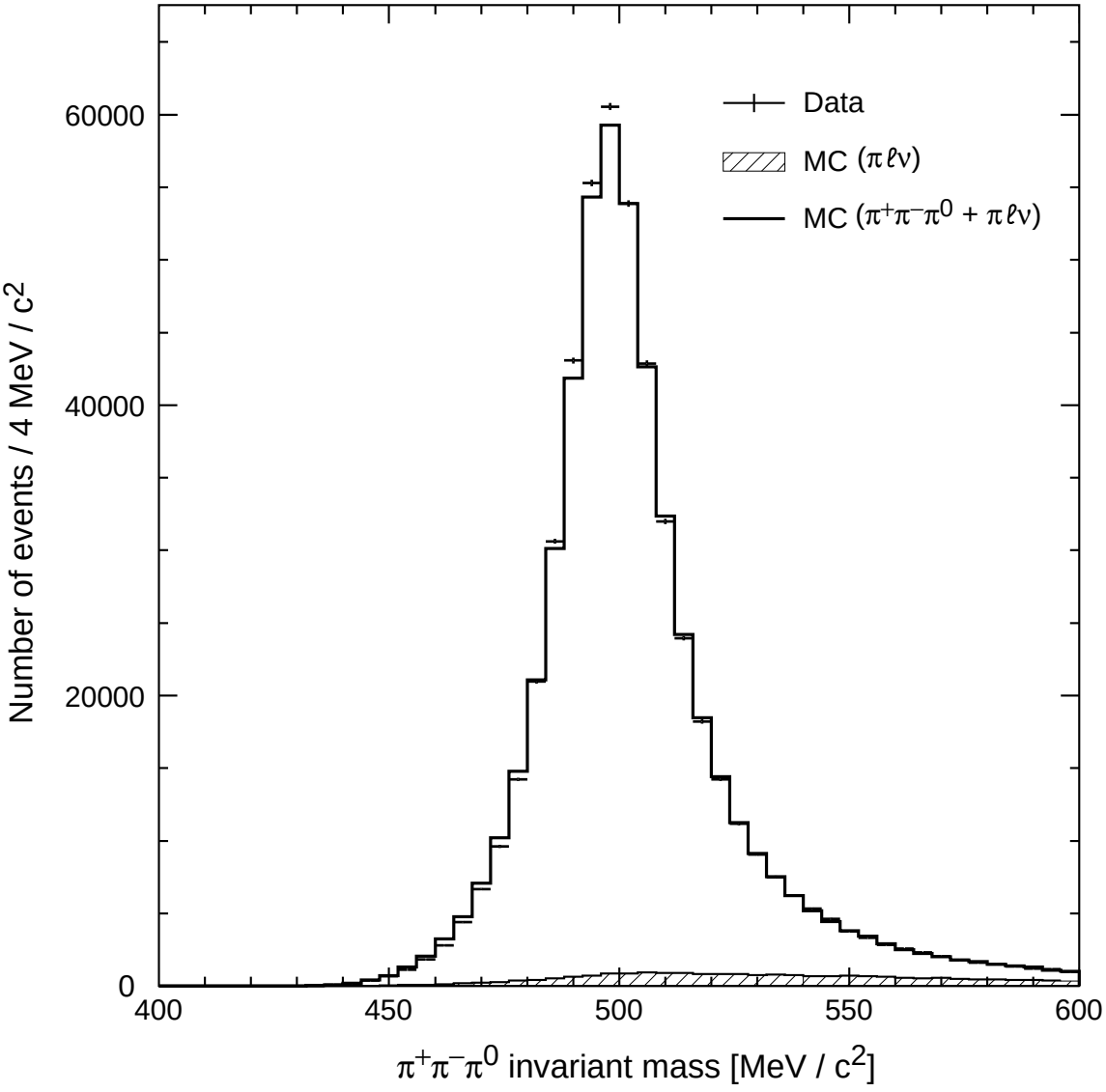

Figure 7: The $\pi^+\pi^-\pi^0$ invariant mass distribution for real and simulated data after the full selection, computed with momenta resulting from our track-fit procedure. The π^0 momentum is defined as the total missing momentum in the $\overline{\mathrm{p}}\mathrm{p}$ annihilation. The plain histogram shows the simulated distribution built from the $\pi^+\pi^-\pi^0$ and the semileptonic decays of neutral kaons, normalized to the real data set above 6 τ_{S}. The background contribution due to semileptonic decay events alone is given by the shaded area.

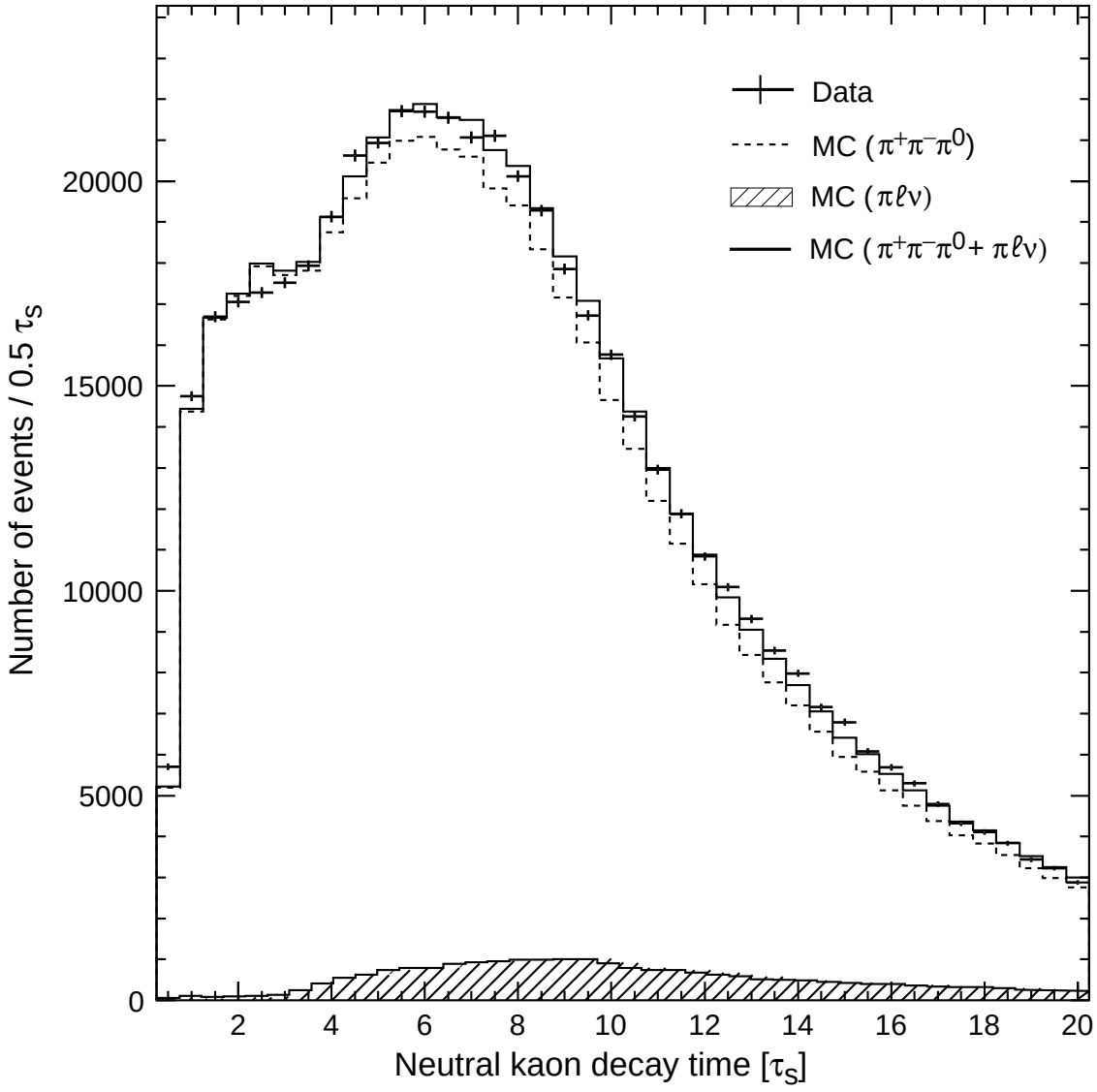

Figure 8: The decay-time distribution of the sum of initial K^0 and $\overline{\mathrm{K}}^0$ decaying into $\pi^+\pi^-\pi^0$ for real and simulated data after applying the final selection. The full line shows the simulated distribution built from the sum of the $\pi^+\pi^-\pi^0$ and the semileptonic decays of neutral kaons, normalized to the real data set above 6 τ_S. The distribution of the signal events is shown by the dashed line, while the background contribution from the semileptonic events is given by the shaded area.

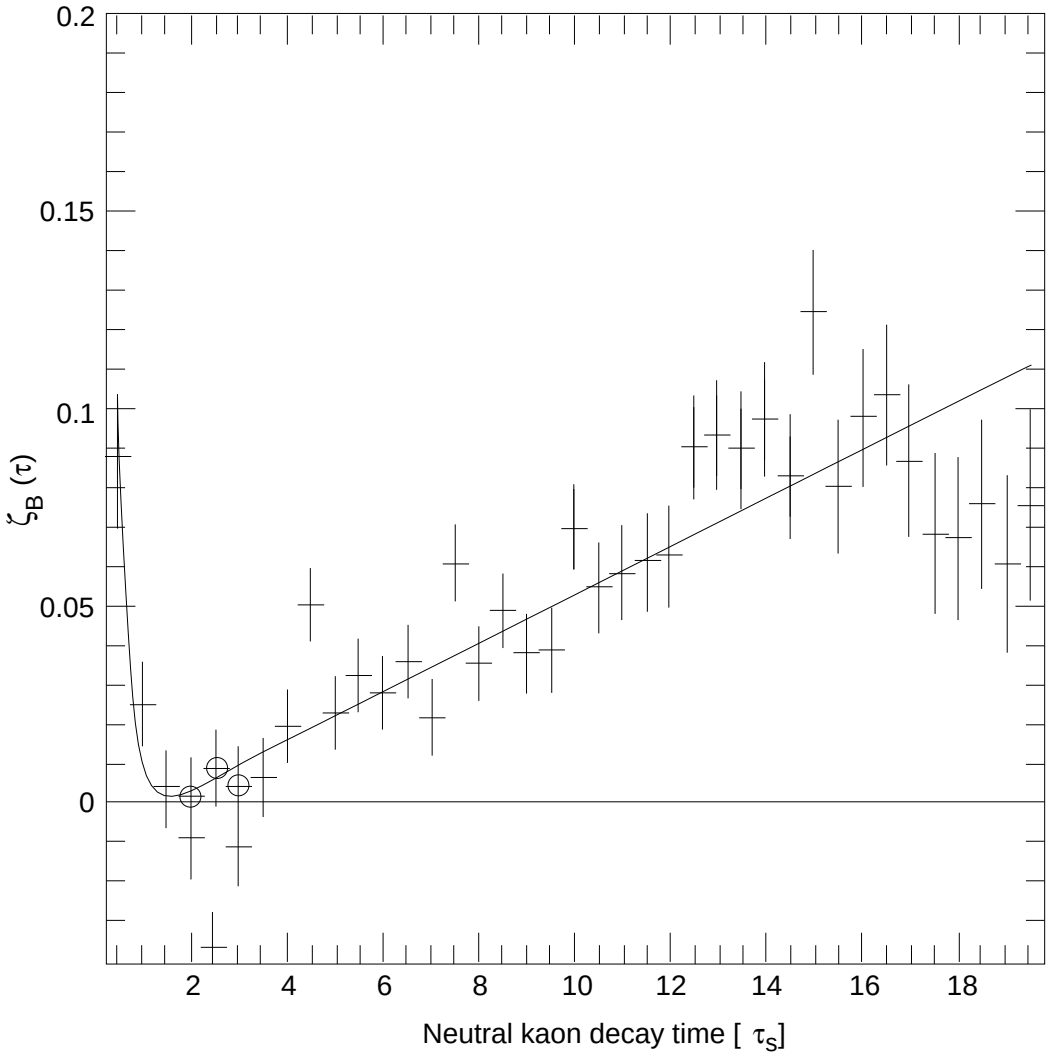

Figure 9: The total-background fraction $\zeta_{\rm B}(\tau)$ (+), defined as the relative difference between real data and simulated $\pi^+\pi^-\pi^0$ data (normalized above 6 $\tau_{\rm S}$). The solid line results from the fit with a parametrization consisting of a linear term, describing the semileptonic contribution, and an exponential term, which accounts for the short decay-time residual background. The analytic shape of $\zeta_{\rm B}(\tau)$ is used when fitting the asymmetries to data. Also shown are the values ($\circ$) obtained after retuning the chamber simulation (see text).

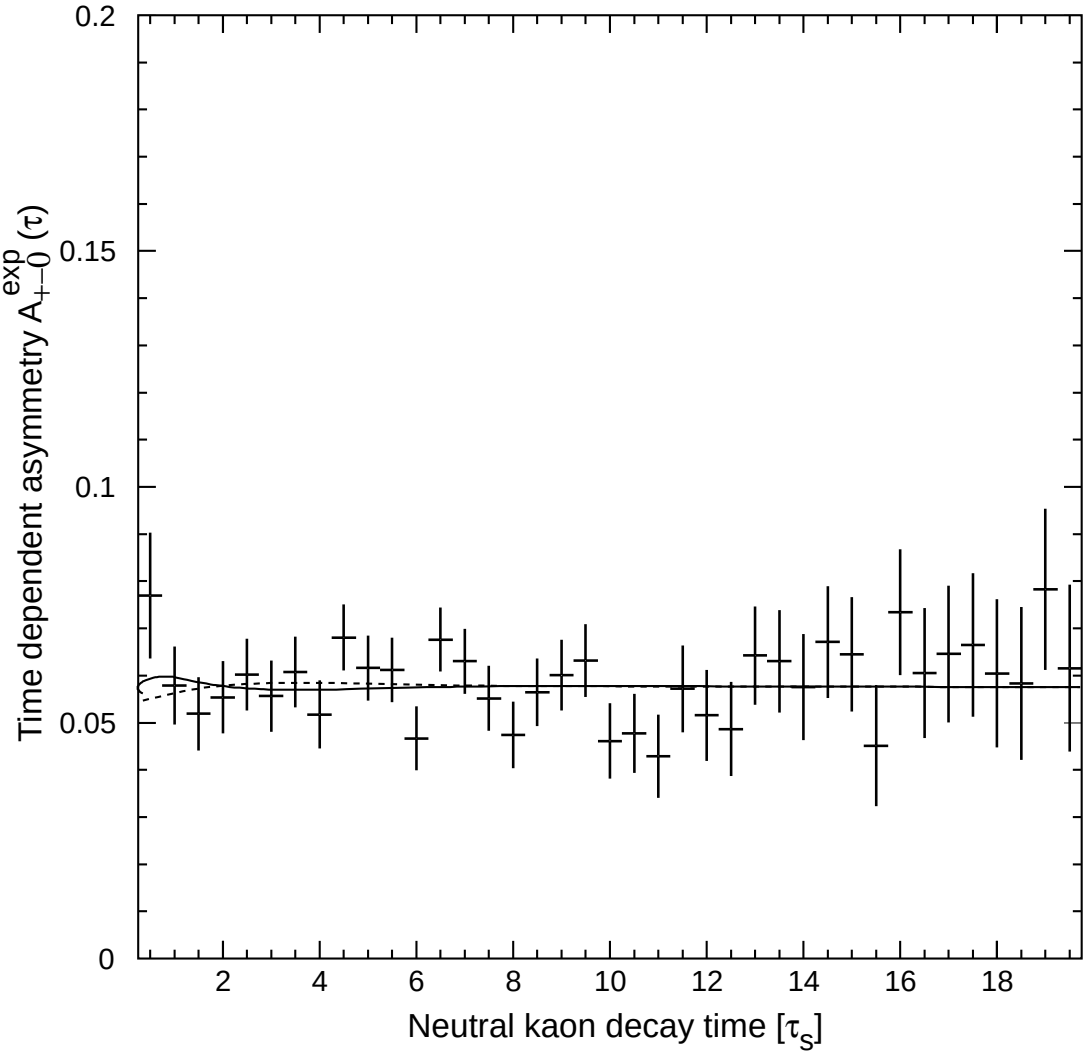

Figure 10: The measured CP-violating decay-rate asymmetry between 0.25 and 19.75 τ_{S}. The solid line is obtained by fitting Eq. (15) to the data. The broken line shows the asymmetry expected when assuming $\eta_{+-0} = \eta_{+-}$.

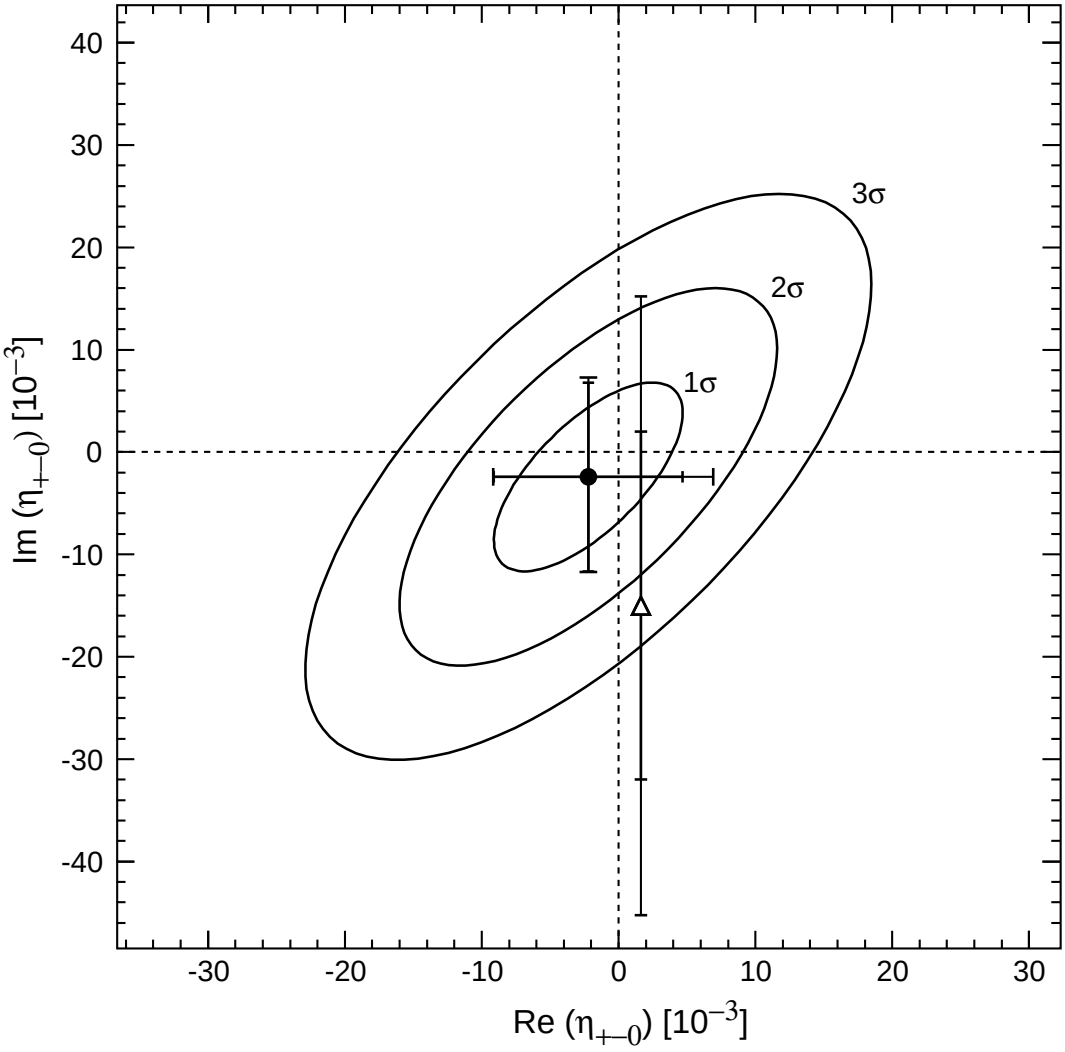

Figure 11: The real and imaginary parts of η_{+-0}: the central value ($\bullet$) with its statistical and total uncertainties, and the statistical correlation ellipses as obtained in this work. For comparison, the result of Zou et al. [21] on $\mathrm{Im}(\eta_{+-0})$, obtained by fixing $\mathrm{Re}(\eta_{+-0}) = \mathrm{Re}(\varepsilon)$, is also shown ($\triangle$) with its statistical and total errors.

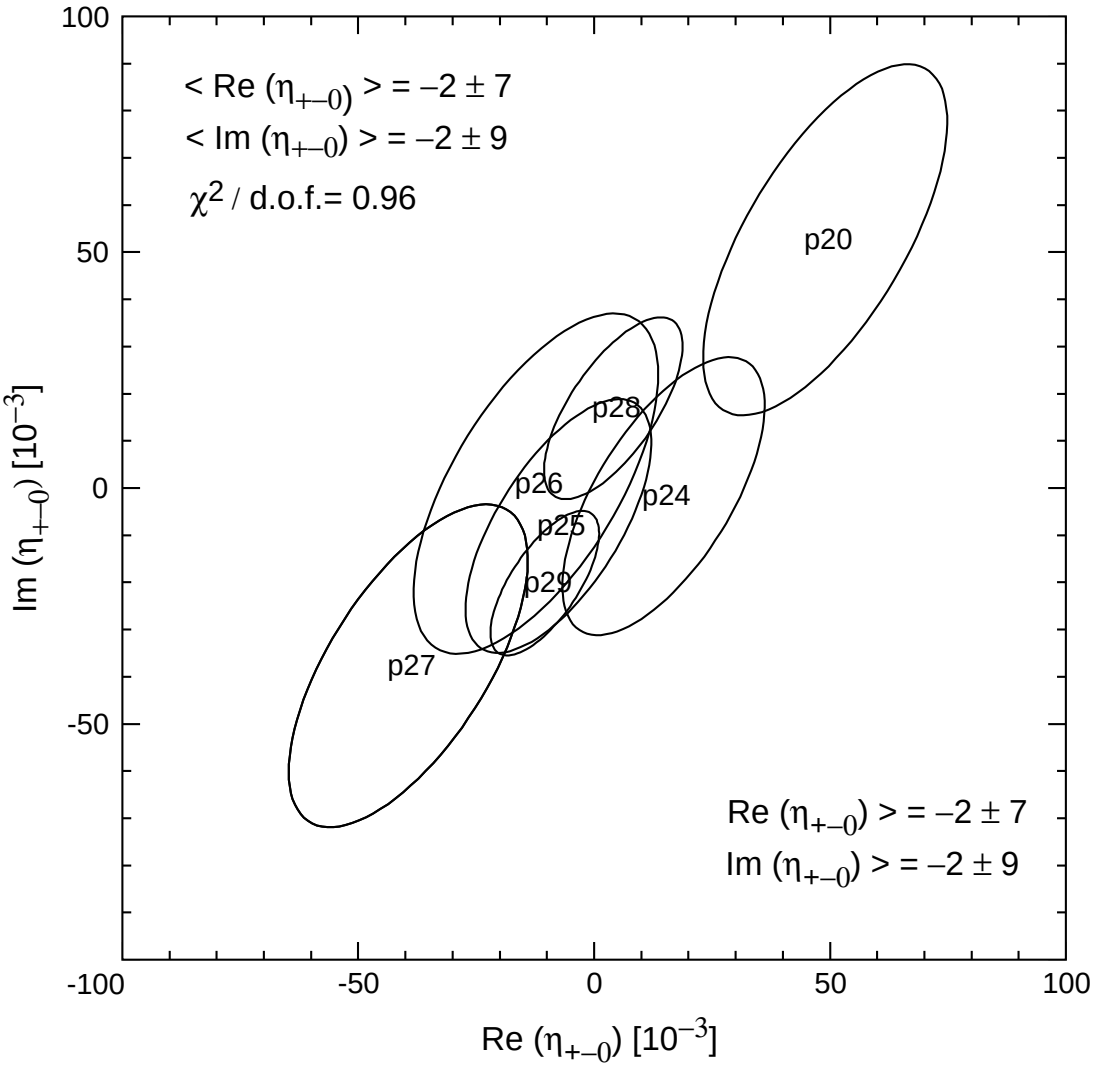

Figure 12: The values of $\mathrm{Re}(\eta_{+-0})$ and $\mathrm{Im}(\eta_{+-0})$ fitted for each data-taking period (p20, p24–p29) and the resulting mean values. The plot shows the projection of the measured values in the complex plane with their statistical correlation ellipses. The area of the ellipses depends on the recorded statistics. The mean values obtained are given in the top left corner and the values of the standard analysis in the bottom right corner.

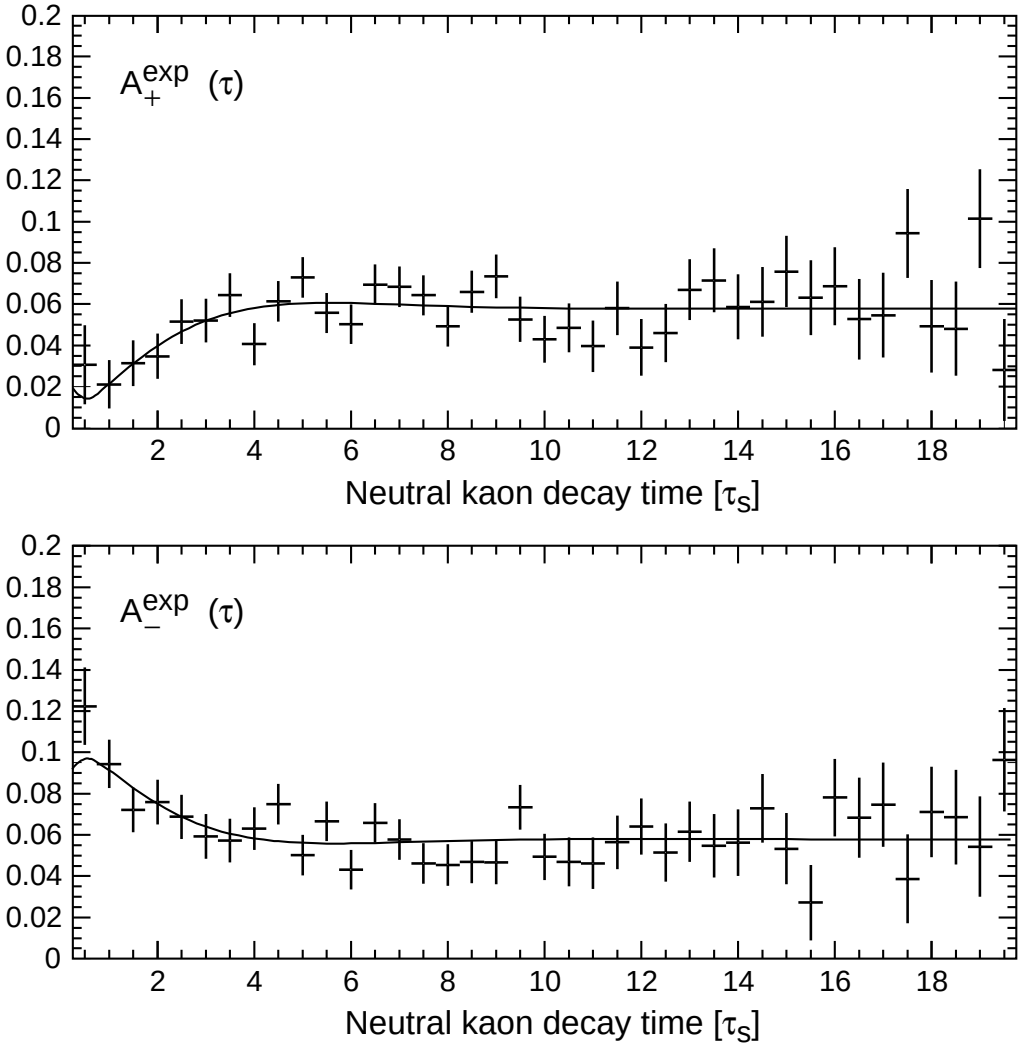

Figure 13: The measured decay-rate asymmetries for $X > 0$ and $X < 0$ between 0.25 and 19.75 τ_S. The solid curves are the result of the simultaneous fit of Eq. (15) assuming common λ and ξ. In this determination, we fixed $\eta_{+-0} = \eta_{+-}$.

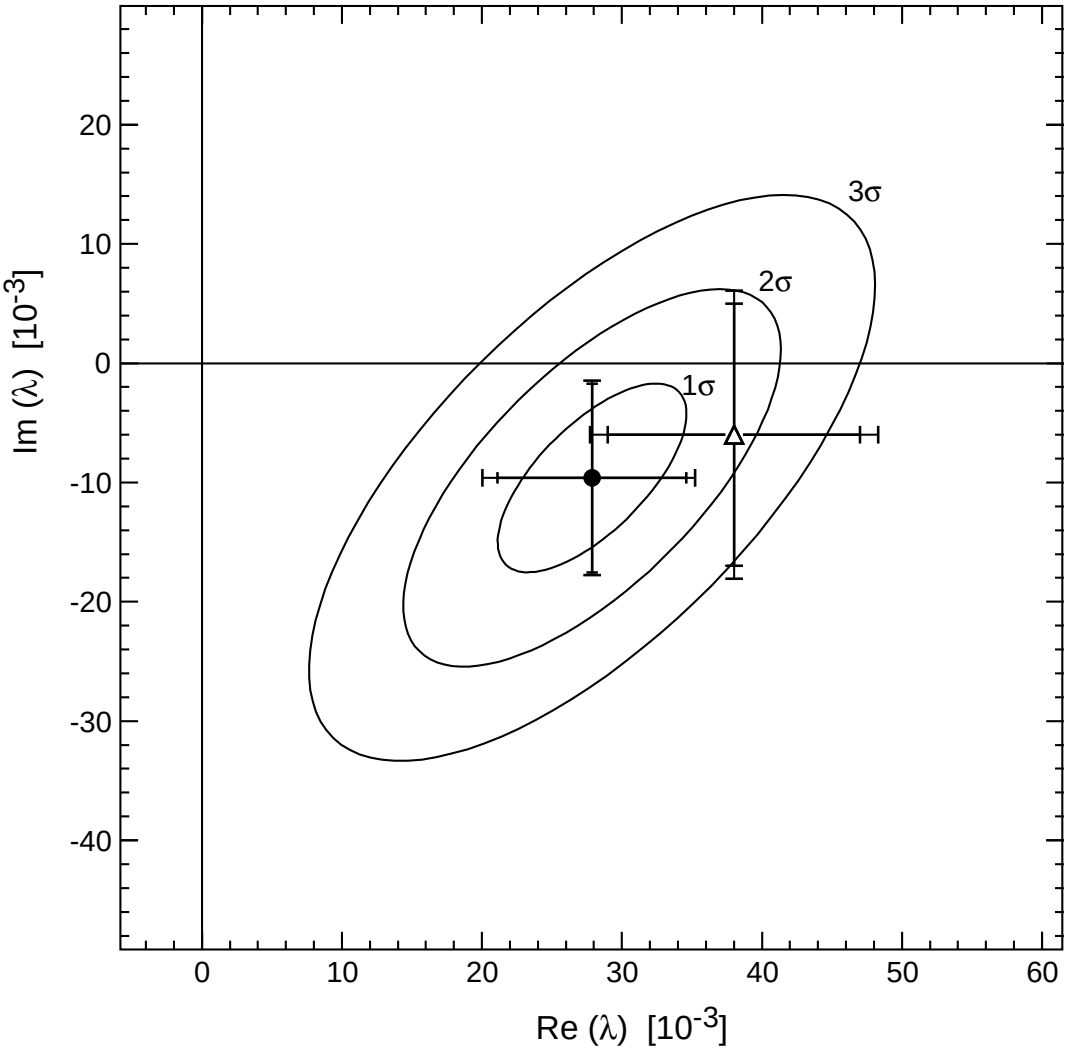

Figure 14: The real and imaginary parts of λ: the central value $(\bullet)$ with its statistical and total uncertainties, and the correlation ellipses as obtained in this work. For comparison, the result of Zou et al. [22] is also shown $(\triangle)$ with its statistical and total error.

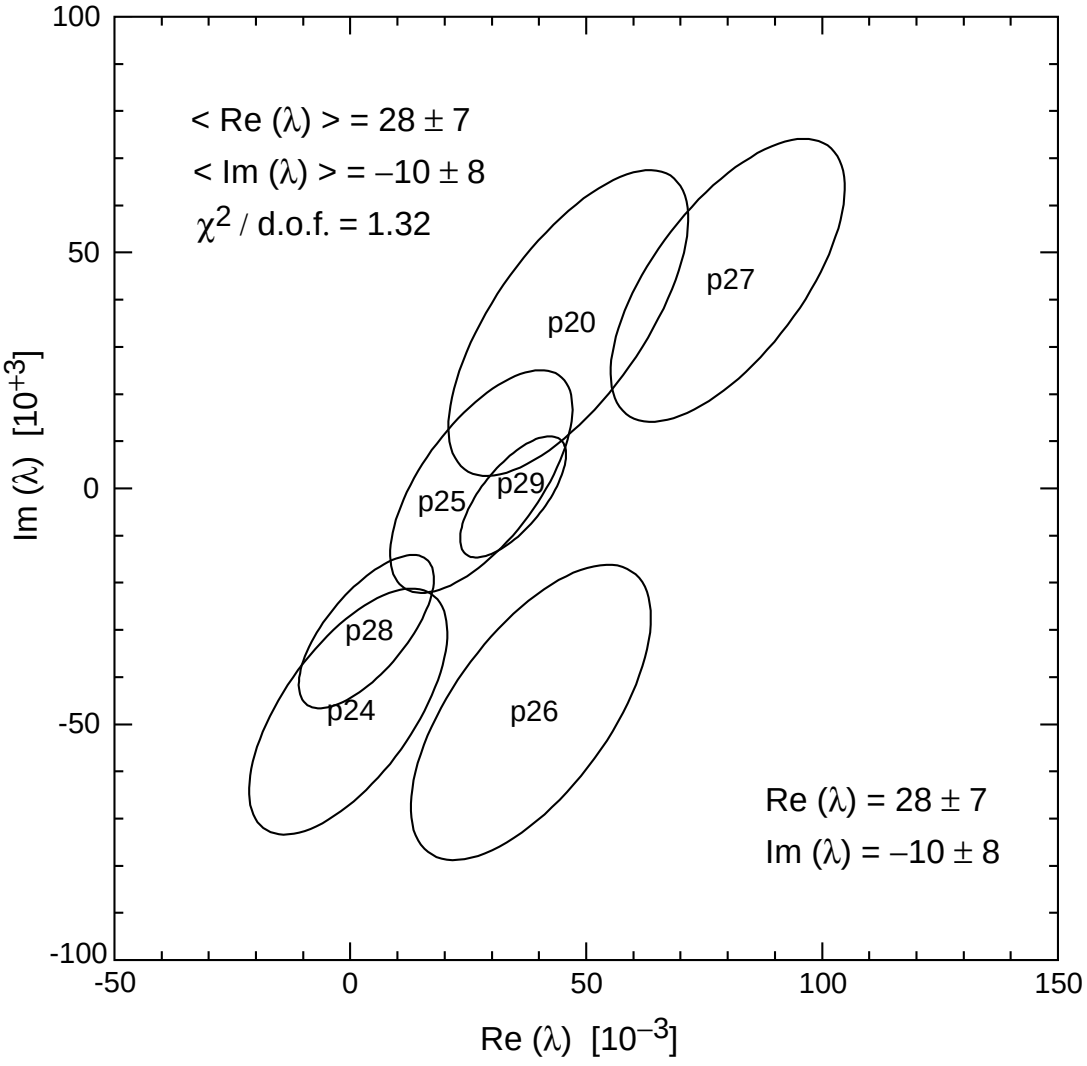

Figure 15: The values of $\mathrm{Re}(\lambda)$ and $\mathrm{Im}(\lambda)$ fitted for each data-taking period (p20, p24–p29) and the resulting mean values. The plot shows the projection of the measured values in the complex plane with their statistical correlation ellipse. The area of the ellipses depends on the recorded statistics. The mean values are given in the top left corner and the values of the standard analysis in the bottom right corner.

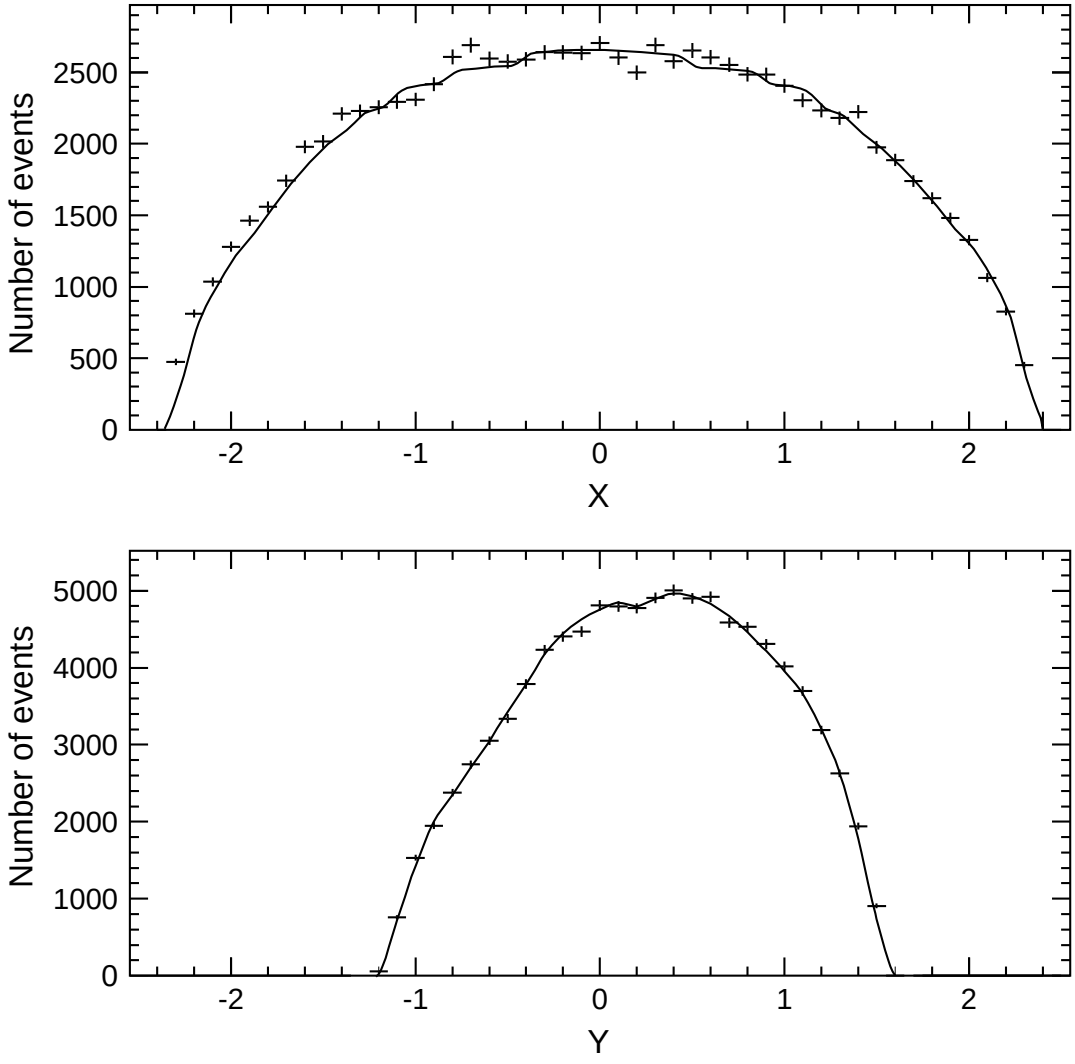

Figure 16: X and Y distributions for $\mathrm{K_L} \to \pi^+\pi^-\pi^0$ decays with a decay time above 2 τ_S. The crosses indicate the data while the solid lines are calculated with the results of the slope-parameter fit.